2020

OIL/WATER NANOEMULSION BIODISTRIBUTION IN MICE UPON INTRAVENOUS ADMINISTRATION

Jiayi Chen
Saint John's University, Jamaica New York

OIL/WATER NANOEMULSION BIODISTRIBUTION IN MICE UPON INTRAVENOUS ADMINISTRATION

A dissertation submitted in partial fulfillment

of the requirements for the degree of

DOCTOR OF PHILOSOPHY

to the faculty of the

DEPARTMENT OF PHARMACEUTICAL SCIENCES

of

COLLEGE OF PHARMACY AND HEALTH SCIENCES

at

ST. JOHN'S UNIVERSITY

New York

by

Jiayi Chen

Date Submitted _____ Date Approved _____

Jiayi Chen

Jun Shao

ABSTRACT

OIL/WATER NANOEMULSION BIODISTRIBUTION IN MICE UPON INTRAVENOUS ADMINISTRATION

Jiayi Chen

The present study aimed to explore the biodistribution of O/W nanoemulsions (NE) upon intravenous administration. Three NEs were prepared with distinctive droplet sizes: SE (29 ± 1 nm), ME (214 ± 2 nm) and LE (883 ± 16 nm) without overlapping of the size distribution. Kolliphor® HS15 was used as the only surfactant for these three NEs, so that their droplets had similar surface structure. The NEs droplet size was stable under room temperature for minimum 3 days in phosphate buffer saline (PBS) and in mice plasma *in vitro* for 4-hour at 37°C. A lipophilic fluorescent dye, 1, 1'-dioctadecyl-3, 3, 3', 3'-tetramethylindocarbocyanine perchlorate (DiI) was selected as the probe and loaded in the SE, ME and LE (designated thereafter as DSE, DME and DLE, respectively). A fluorometry for DiI was established with a linear range of 1.0-1000 ng/mL.

The processing procedure and assay method for biological samples were developed. DiI extraction efficiency was 74.6-93.4%, depending on the tissues. For the biodistribution study, tumor-bearing mice received intravenous injection of DiI (2-5 mg/kg) in free solution (DS) or in the NEs via tail vein. The mice were sacrificed at sampling time points and the biological samples were assayed for DiI concentrations. DS manifested early tissues peak concentration (apparent T_{max}s at 0.5 h) followed by rapid decline, with

tissue recovery mainly from the liver, spleen and lungs. DSE had a comparable plasma profile as DS but lower concentrations in the spleen and lungs as compared to the corresponding tissue profiles followed by the administration of DS. DME showed a sustained plasma circulation and a long-term non-specific higher tissue uptake with significant accumulation in the heart, lung, liver and spleen. DLE displayed a favorable accumulation in the RES organs including the lung, spleen, and liver. In conclusion, the present study demonstrates that O/W NE exhibits altered biodistribution upon intravenous administration. And these features may be utilized as a targeted drug delivery and drug redisposition strategy.

DEDICATION

I DEDICATE THIS WORK TO MY BELOVED PARENTS (XIUBAO LU AND JUNYU CHEN), WIFE (JIAO WU) AND FAMILY FOR THEIR ENDLESS LOVE, SUPPORT AND ENCOURAGEMENT.

ACKNOWLEDGEMENTS

This dissertation would have been impossible without the unconditional support from many individuals and I am grateful to all of them.

Foremost, my mentor, Dr. Jun Shao, who has not only been my research mentor, but also a godly mentor of my life. Along with my master's and doctoral study, his academic knowledge and Christianity belief have taught me critical thinking and the true meaning of my life. I would like to thank him for all his everlasting guidance and patient support.

Special appreciation is extended to the members of my committee: Dr. Zhesheng Chen, Dr. Senshang Lin, Dr. Abu Serajuddin and Dr. Emilio Squillante who provided countless valuable comments. Their generous contribution of time and knowledge helped make this achievement possible. I would also thank Dr. Blase Billack, Dr. Ketankumar Patel, Dr. Vivek Gupta, Dr. Enju Wang, Dr. Ashley Martino, Dr. Woon-Kai Low and Dr. Tanaji Talele for their tremendous help, advice and research facilities.

I am grateful to the entire Dean Office, Department of Pharmaceutical Sciences, Animal Care Center and Science Supply for providing me the financial support and technical assistance.

I must also express my gratitude to my lab mates (Mayuri, Pulkit, Darshana, Prachi, Kanyaphat, Atanu, Yuxing and Yeqing) for being a continuous source of encouragement, inspiration and friendship.

My family deserves a special recognition. My parents (Xiubao Lu and Junyu Chen) have raised and taught me to be who I am through their endless love. My wife (Jiao Wu) has been and will ever be supporting and companying me through my life. My daughters (Ruthie Chen and Rachel Chen) were the precious gifts from the God who have brightened and filled my life with joy. My parents-in-law (Lianzhen Feng and Chunde Wu) have helped me tremendously especially after I had two daughters. My family aunties and uncles (Xiudi Lu and Zhongde Wang; Jin Lin and Junlin Chen) have also supported me continuously and unconditionally in my daily life throughout my doctoral study.

Last but not least, I would like to thank my heavenly Father and Jesus my savior. I could never have lived such a life filled with love without the grace from them, neither would I ever live a life full of hope, peace and faithfulness without knowing them.

TABLE OF CONTENTS

LIST OF TABLES

LIST OF FIGURES

NOMENCLATURE AND ABBREVIATIONS

ANOVA	Analysis of variance
AUC	Area under the curve
C_{max}	Maximum concentration
CI	Confidence interval
CL	Clearance
CM	Complete medium
CNS	Central nervous system
CT	Computed tomography
DDS	Drug delivery system
DiI	1,1'-dioctadecyl-3,3,3',3'-tetramethylindocarbocyanine perchlorate
DLE	DiI loaded large-size nanoemulsion
DLS	Dynamic light scattering
DME	DiI loaded medium-size nanoemulsion
DMSO	Dimethylsulfoxide
DSE	DiI loaded small-size nanoemulsion
EA	Ethyl Acetate
Em.	Emission
EPR	Enhanced permeability and retention
Ex.	Excitation
FDA	The Food and Drug Administration
FITC	Fluorescein Isothiocyanate
GRAS	Generally recognized as safe
HBSS	Hanks' balance salt solution
HLB	Hydrophile-lipophile balance
HS	Kolliphor® HS 15
i.v.	Intravenous
LBDDS	Lipid-based drug delivery system
LE	Large-size nanoemulsion
LY	Lucifer Yellow
MCM	Capmul® MCM NF
MCT	Medium chain triglyceride
ME	Medium-size nanoemulsion
MPS	Mononuclear phagocyte system
MRT	Mean residence time
MW	Molecular weight
NCI	The National Cancer Institute
NE	Nanoemulsion
NCE	New chemical entity
NIH	The National Institutes of Health
O/W	Oil in water
PBS	Phosphate buffer saline
PEG	Polyethylene Glycol
PI	Polydispersity index
PK	Pharmacokinetics
RES	Reticuloendothelial system
RSD	Relative standard deviation
SD	Standard Deviation
SE	Small-size nanoemulsion
SEM	Standard error of the mean
W/O	Water in oil
WL	Labrafac™ Lipophille WL1349

Chapter 1. Introduction

In this chapter, the following topics are elaborated:

- How the research idea was formed
- The literature search and the refinement of the research goals
- The hypothesis, objective and specific aims

1.1. The formation of the research idea

Since the emerge of nanotechnology, many scientific areas have benefited significantly from its introduction and revolution. For the field of biomedicine and pharmaceutical sciences, though mentions of nanoparticles could be traced back as early as late 1970s, the term nanomedicine appeared much later at the turn of last century (Astruc, 2015). It was even later in 2005 when the term was first clearly defined by the European Science Foundation as "*Nanomedicine uses nano-sized tools for the diagnosis, prevention and treatment of disease and to gain increased understanding of the complex underlying patho-physiology of disease. The ultimate goal is to improve quality of life.*" (European Science Foundation, 2005) The applications of nanotechnology were further categorized into three areas of diagnosis, imaging agents and drug delivery with nanoparticles (NP) in the size range of 1-1000 nm (Peer et al, 2007). Despite the relative short history of biomedical applications of the technology, the growth of academic and clinical research interest in nanomedicine has been explosively blossoming, resulted in tens of thousands publications per year over the last decade. Nanomedicine holds such an enormous promise for healthcare that in the United States, the National Institutes of Health (NIH) has

continuously increased their annual funding to Research Project Grant Program (R01) focused on nanomedicine ever since 2009, with more than $130 million invested in 2018 alone. It also fostered several special initiatives/programs such as the National Cancer Institute (NCI) to facilitate clinical translation of nanomedicines (He et al., 2019).

However, regardless of the tremendous investments and efforts spent, accumulatively there were only 50 approved nanodrug products by the FDA as of year 2017 (Ventola, et al., 2017), among which polymeric, liposomal and nanocrystal formulations were heavily represented. The extreme high attrition rate for nanodrugs was attributed to multiple folds of reasons, of which the hardness of characterizations, insignificantly improved efficacy, safety issues, complexity in manufacturing, cost-benefit considerations, etc. all pose barriers to the survival of nanodrugs against their conventional competitors (Kola and Landis, 2004).

In such context, a nanoplatform would be highly desired if it could address some of the aforementioned obstacles. Indeed, a relative new nano-sized formulation strategy: nanoemulsion (NE), has attracted more and more research interest. NEs are oil-in-water (O/W) or water-in-oil (W/O) dispersion of two immiscible liquids stabilized by an appropriate surfactant with or without other excipients. It is sometimes used interchangeably with submicron emulsion or mini emulsion to distinguish from coarse/macro emulsions which have larger droplet sizes over 1 micron, yet on the other hand differentiate from microemulsions which differ tremendously in structural aspects and long term thermodynamic stability (McClements, 2012; Singh et al., 2017). NE provides a wide spectrum of formulation advantages such as the enhancement of lipophilic drug payload and oral bioavailability, ease of preparation and scale-up, exclusiveness of organic solvents and use of Generally Recognized as Safe (GRAS) materials, etc. Extensive researches have been conducted to exploit NE by various delivery routes including oral (Soliman et al., 2016), parenteral (Venkateshwarlu et al., 2010), topical (Hagigit et al., 2010) and intranasal

(Shobhit et al., 2016). Currently, a few NE drug products have been approved by the FDA (Ganta et al., 2014) while numerous are still undergoing clinical trials (Singh et al., 2017).

Quoted from Rivera, a nanomaterial should possess properties which neither the bulk material nor the atoms or molecules of that same material display. Essentially, nanodrugs are "*pharmaceuticals engineered on the nanoscale, i.e., pharmaceuticals where the nanomaterial plays the pivotal therapeutic role or adds additional functionality to the previous compound*". (Rivera et al., 2010) In this sense, as a nanomaterial, NE could possibly alter drug pharmacokinetics (PK) profile and/or redisposition in the organ/tissue as compared to the corresponding free drug solution after intravenous (i.v.) administration.

Indeed, our interest on the potential of NE to alter PK and biodistribution was inspired by two cases, the first one being the success of the well-known nanodrug product Doxil® (Doxorubicin Hydrochloride liposome injection). Doxorubicin has been an anthracycline drug effective for a variety of cancers but its cardiotoxicity had held back its use (Alexander et al., 1979). By loading the drug into liposomes, Doxil® significantly reduced Doxorubicin cardiotoxicity by the elimination of the intensive peak concentration in the heart, which eventually granted its approval by the FDA (Papahadjopoulos et al., 1991). In fact, many nanodrug products gained approval not by the enhancement of drug efficacy, but because of the reduction of drug or excipients related side effects of conventional formulations. The second case is the discovery of the enhanced permeability and retention effect (EPR), of which the centric principle was based on molecule/particle size. Briefly, Yasuhiro Matsumura and Hiroshi Maeda found that radioactive protein with molecular weight (MW) over 65,000 preferably accumulated in tumor tissues compared with protein with MW 12,000 after intravenous injection to tumor bearing mice (Matsumura and Maeda, 1986). This phenomenon, due to the unique tumor physiological properties: hyper-vasculature, enhanced vascular permeability and little recovery of the

macromolecules via the blood vessels and lymphatic system, was subsequently utilized as the tumor passive targeting strategy (Maeda et al., 2013) and has been guiding the development of nanoparticulate drug delivery system (DDS) ever since, though it has become controversial more recently (Prabhakar et al., 2013; Nicholas and Bae, 2014).

Therefore, it would be meaningful to investigate whether NE could alter encapsulated drug substances' PK and biodistribution, and whether the NE droplet size played a role in such change. A direct way to address the problem is to administer NEs with different droplet size intravenously to investigate the biodistribution. Should the assumption be true, it could be utilized as a targeted drug delivery and drug redisposition strategy to increase efficacy and/or to reduce off-target organs toxicities. These potential benefits set up the premise for the current study.

1.2. The literature search and the refinement of the research goals

When we dig into the literature, we found numerous size-dependent biodistribution studies such as polymeric NP (He et al., 2010), gold NP (Perrault et al., 2009), liposome (Liu et al., 1992) and quantum dot (Popović et al., 2010), etc. The results from other nano DDS have confirmed that the particle size is one of the major factors which governed the nanomaterials *in vivo* biodistribution. Surprisingly, despite the recent blossoming research interests on NEs, studies of NE biodistribution were quite scattered and for those focusing on the droplet size effect were further limited.

One of the studies on NE droplet size effect on biodistribution was conducted by Attia et al. (Attia et al., 2015). In their work, NE with mean droplet size of 55 and 100 nm were prepared by use of the same lipid and surfactant at different percentage composition. Their findings suggested that 55 nm NE was less uptaken by hepatocytes and macrophages *in vitro*, and less toxic to the

mice *in vivo* which was demonstrated by the longer survival time after intravenous administration. The authors attributed this decreased *in vivo* toxicity to the reduced cellular uptake. Notably, no size-dependent impact of NE on biodistributions was observed based on the plasma, liver, spleen and kidneys profiles. Nevertheless, this conclusion was questionable because the two NEs size distributions significantly overlapped with each other, which very likely caused the similar *in vivo* tissue profiles.

Another study by Chen and coworkers (Chen et al., 2016) used iodinated NEs with 25, 60 and 100 nm droplet size to investigate the size-dependent NE biodistribution. Similar cellular uptake results were observed that increased size caused increased phagocytic uptake. The *in vivo* computed tomography (CT) results after intravenous administration of NEs demonstrated enhanced liver and spleen accumulation as the increase of the size.

Based on what have been reported in the literature, we speculated that NE droplet size should have impact on their *in vivo* biodistributions like the other nanomaterials. However, this effect has not been clearly elucidated because of two reasons. First, the mean droplet size of the NEs studied were selected too close which posed the argument that the similar biodistribution could be due to the essentially no-significantly-different sizes in the *in vivo* environment. Secondly, the droplet size studied were no more than 100 nm which left the vacuum of the knowledge about the bigger size. Besides the liver and spleen, the lungs are also main constitution of the reticuloendothelial system (RES) in the body which is responsible to uptake particulate matters (Saba, 1970). Therefore, larger nanoparticles could also see preferable dispositions in the lungs (Blanco et al., 2016). To more clearly address the problem, an extended span of NE droplet size became necessary. Hence, a reasonable approach is to develop NEs with droplet size towards the two-end of the submicron range, i.e., less than 50 nm and close to 1 micron, and an intermediate size in between. However, unlike solid nanoparticles, the liquid droplets usually present much less

precise sizes, and this phenomenon would be further magnified as the mean droplet size of NE increases. According to our preliminary data, the mean droplet size of a certain NE did not necessarily correlate with its actual size distribution, usually due to multi-modal distribution or a wide unimodal distribution. In addition, the increased size also deteriorated the stability of NEs significantly. All these factors could probably explain the remarkable limitations of the previous studies on the size effect of NEs as compared to the studies on the size effect of solid nanoparticles.

To put in short, the present research goal was refined as to focus on the development of more defined droplet size NEs with narrow size distribution which significantly differs from each other in the sub-micron range, and to investigate the droplet size impact on their *in vivo* biodistributions.

1.3. The hypothesis, objective and specific aims

Our hypothesis was that O/W NEs could alter encapsulated drug biodistribution and such alteration was impacted mainly by the droplet size of the NEs.

To test the hypothesis, the overall objective of the study was to develop O/W NEs with significantly different droplet size and similar droplet surface structure, and to compare their *in vivo* biodistributions. The specific aims of the study were as follows:

1. To prepare O/W NEs which have distinct size (<50 nm for the small-size NE (SE), ~200 nm for the medium-size NE (ME) and ~1 micron for the large-size NE (LE)) with narrow size distribution.
2. To evaluate the prepared NEs stability for their suitability for the *in vivo* study.

3. To identify an agent to label the NEs.
4. To validate the assay method for the labeling agent.
5. To establish a tumor-bearing animal model for the *in vivo* study.
6. To establish the *in vivo* biological sample preparation and assay protocol.
7. To study and compare the biodistribution of labeled NEs with distinct droplet sizes after intravenous administration.

Specific Aims 1-2 regarding the preparations and characterizations of the NEs are addressed in Chapter 2. Specific Aims 3-6 are addressed in Chapter 3, and Specific Aim 7 of the *in vivo* assessments is elaborated in Chapter 4. Finally, in Chapter 5 the entire study is summarized together with a few insights and discussions.

Chapter 2. Preparation and evaluation of nanoemulsions with distinct droplet sizes

In this chapter, the following topics are addressed:

- The preparation of O/W NEs with distinct droplet size and narrow size distribution
- The stability of the prepared NEs under certain conditions

2.1. Introduction

The preparation methods for NE can be categorized into high-energy method, low-energy method, and a combination of the two (Mason et al., 2006). Low-energy method usually produces ultra-fine droplets, and it is generally limited by oil type and emulsifiers that can be used. It can be further classified as spontaneous emulsification (Bouchemal et al., 2004) and phase inversion (Fernandez et al., 2004). High energy method, on the other hand, depends on mechanical devices to create disruptive forces for size reduction, which is usually implemented by ultra-sonicators, high pressure homogenizers or microfluidizers. This method is more versatile in which almost any kinds of oils and emulsifiers can be subjected to nano-emulsification. However, the major limitation lies in the instrumental cost and the generation of high operational temperatures which rules out thermolabile drugs (Singh et al., 2017).

2.2. Preparation of O/W NEs with distinct droplet size

2.2.1. Materials and methodology

Captex® 8000 (C8 triglyceride), Captex® 1000 (C10 triglyceride), Capmul® MCM NF (C8/C10 monoglyceride) were kind gifts from Abitec Corporation (Abitec, WI). Labrafac™ Lipophille WL1349 was a kind gift from Gattefosse Corporation (Gattefosse, NJ). Kolliphor® RH 40, Kolliphor® HS 15, Tween® 80 were purchased from Sigma-Aldrich (St. Louis, MO). Soybean oil (Spectrum, NJ), Pluronic F68 (BASF, NJ) and soybean lecithin (Alfa Aesar, MA) were purchased through VWR.

To prepare the NEs with desired droplet size and size distribution, commonly used medium chain mono-/di- and triglycerides, long chain triglycerides and commercially available surfactants were screened with an emphasis on GRAS ingredients. For the SE, low energy preparation method was applied. Briefly, predetermined amount of lipid(s) and surfactant were mixed at 50°C, 300 rpm for 2 h to ensure homogeneous preconcentrate (MaxQ 4000, Thermo Fisher Scientific, MA). The preconcentrate was cooled down to 37°C prior to be mixed with 37°C distilled water (1:4 w/v). The SE was obtained by gently shaking the mixture.

For the ME and LE, high energy preparation method was utilized. The preparation procedures included homogenization and/or ultrasonication individually or in combination. Processing parameters such as homogenization speed (5000, 10,000 and 20,000 rpm) and time (2, 5 and 10 min), and ultrasonication amplitude (20, 30 and 40%), on-duty/rest cycle pattern and on-duty duration (2 to 6 min) were evaluated. Lipid(s), surfactant, and distilled water were first weighed and homogenized at 30 °C with various speed and time to produce coarse emulsion (VirTis Tempest I.Q.^{2}, SP Scientific, PA). The coarse emulsion was subsequently ultrasonicated at

various amplitude for different period of on-duty time, with a 10 s/10 s on-duty/rest cycle. Ice bath was applied to prevent excessive heat generated during the process (Cole Parmer, IL).

The prepared NEs were properly diluted before droplet size and polydispersity index (PI) determination by dynamic light scattering (DLS, Zetasizer Nano ZS, Malvern, U.K.).

2.2.2. Results and discussions

A variety of commercially available lipids (medium chain mono/di-glyceride, medium chain triglyceride and long chain triglycerides), surfactants (Polysorbate 80, Poloxamer 188, Polyoxyl (40)-hydrogenated castor oil, Polyethylene glycol (15)-hydroxystearate and soybean lecithin) were screened individually or in combinations. The criteria for the screening included: (1) The capability to produce desired NEs droplet size with narrow distribution; (2) The formulation should be able to solubilize the labeling agent at relevant dose for in vivo application; (3) The surface of the droplets should be similar across different NEs as best; (4) The NEs need to have suitable stability for in vivo assessment; (5) If possible, the ingredients should be approved by FDA for parenteral use or GRAS ingredients and (6) Formulations and preparation should be simple if possible.

Intralipid® was invented by the Swedish physician and nutrition researcher Arvid Wretlind, (Isaksson, et al., 2002). The product gained approval by the Food and Drug Administration (FDA) in 1972 and has been the standard intravenous lipid nutrition medication in the United States to the present. It is comprised of GRAS ingredients, i.e., soybean oil (20%) and egg lecithin (1.2% w/v), with the latter one exhibiting good emulsifying and O/W interface stabilizing effect (Hammond et al., 2005). Besides, the label specifies the mean droplet size of the product of 0.5 micron (Intralipid® 20% I.V. fat emulsion FDA label). All these features made the well-

established Intralipid 20% a reasonable starting point, and the composition of soybean oil and soybean lecithin along with the preparation parameters were adjusted to achieve desired NE droplet sizes. Nevertheless, NEs associated with soy lecithin usually exhibited wide span of size distribution (100 nm to 1 micron) and sometimes produced multimodal rather than monomodal size distribution. The droplet size was neither resistant to the dilution. For example, despite the label claiming a 0.5 micron in size for Intralipid 20%, about 300 nm was observed upon dilution in distilled water through 5- to 500-fold. Furthermore, as a long chain triglyceride, soybean oil may not be the best lipid to solubilize lipophilic drugs as compared to medium chain glycerides (Hippalgaonkar et al., 2010). Subsequently, medium chain mono/di- and triglycerides were tested with some synthetic surfactants, with the centric emphasis being the distribution of the NEs size. As illustrated in **Figure 2.1,** both NEs exhibited similar mean sizes, but none of them could be further considered as they either presented a multi-modal or a wide unimodal distribution. Thereby, rather than simply report the mean droplet size, the individual distribution pattern would actually make more sense in the current study and should be presented instead. However, due to the limited space, the results are summarized in **Table 2.1** in the manner of the range of droplet size and polydispersity index (PI) by the mainly tested ingredients and preparation parameters.

Kolliphor® HS15 (HS, formerly under the name Solutol® HS 15) is a non-ionic surfactant which is frequently used in *in vitro* screening and *in vivo* efficacy studies of poorly soluble new chemical entities (NCE) (Shah et al., 2014). It is synthesized by reacting 12-hydroxystearic acid with ethylene oxide in presence of an alkaline catalyst to yield the major components, polyethoxylated derivatives (~70%) and the minor components (free polyethylene glycol [PEG], ~30%). HS provides profound safety and toxicological profile relatively better than polysorbate 80 and Kolliphor® EL (Wang et al., 2004), which makes it an excellent choice for screening and pre-clinical pharmacokinetic (PK) studies of cytotoxic and oncology drugs among many other

indications (Ali and Kolter, 2019). Furthermore, it is also approved by FDA in injectable and ophthalmic drugs. Besides these unique advantages, more importantly though, when combined with the medium chain triglyceride Labrafac™ Lipophille WL1349 (WL) at various percentage, it produced desired NE droplet size distributions and thus both of them were selected as the final ingredients (**Table 2.2**).

The NEs compositions and preparation methods are summarized in **Table 2.3**. Briefly, for ME and LE preparation, a process of homogenization at 10,000 rpm for 10 min yielded coarse emulsions of large droplet sizes with multiple peaks. The coarse emulsions had extremely limited stabilities that they tended to be phase separated in as short as 15 min. Hence, a subsequent step of ultrasonication was applied to reduce the droplet size and to improve uniformity and stability as well. As the length of on-duty time and the energy input affected the NE droplet size (Delmas et al., 2011), both parameters were evaluated (2, 4 and 6 min for the on-duty time whilst 20, 30 and 40% amplitude for the energy input). The on-duty run for 6 min with 10s/10s cycle at 20% amplitude produced the most uniform NEs of the desired droplet sizes. For SE, Capmul® MCM NF (MCM) was also included to further reduce the droplet size. **Figure 2.2** depicts the merged peaks distribution for one set of SE, ME and LE. They had droplet size distribution of 30 ± 9 nm for SE, 212 ± 64 nm for ME and 893 ± 158 nm for LE, respectively. **Table 2.4** summarizes the droplet size and PI for the triplicate. They had unique droplet distribution which did not overlap with each other. This was of significance because it excluded the potential interferences of the effect from a "mixed" droplet and made it clear to interpret the further in *vivo* data. In addition, since the major surfactant was constant (HS), the effect of surface charge and chain length could also be minimized. (Buszello et al., 2000; Pozzi et al., 2014)

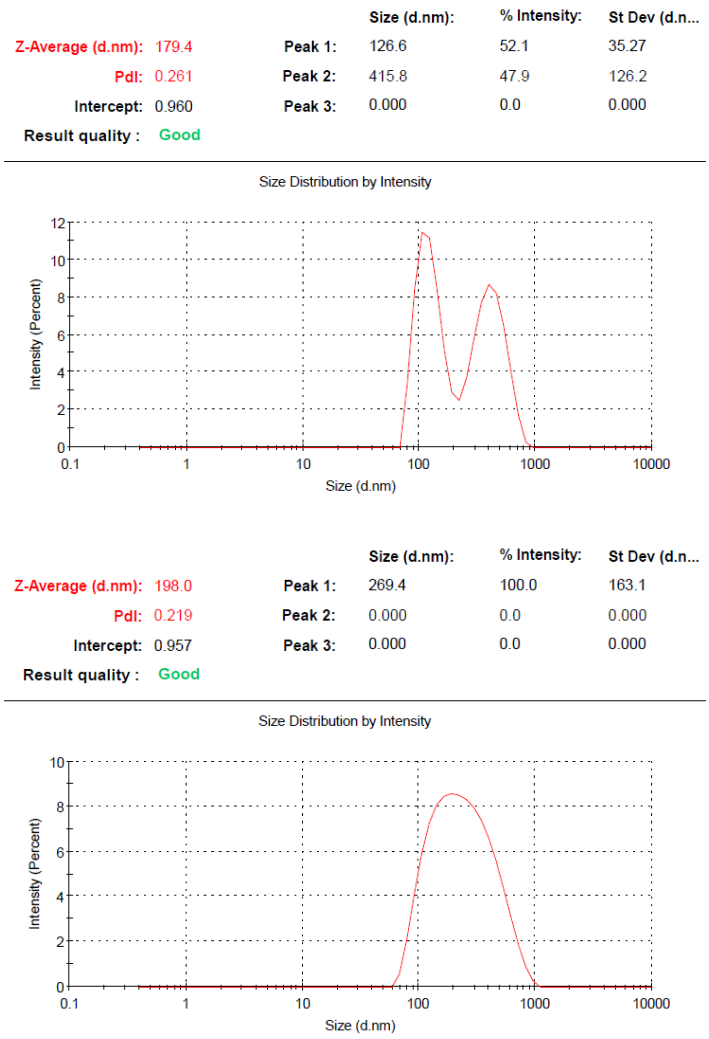

Figure 2.1 The illustration of two NEs with closed mean droplet size yet distinct size distribution pattern.

Table 2.1 The major screened ingredients, processing parameters, and droplet size and polydispersity index range

Lipid/ Surfactant	Homogenization (rpm, time, temperature)	Ultrasonication (Time, Amplitude)	Droplet size (nm)	PI
Intralipid 20%	N/A	N/A	243 – 266	0.08 – 0.15
SO (10-20%) / SL (1.2%)	N/A	5 min, 40%	162 – 170	0.18 – 0.26
SO (20%) / SL (1.2%)	275 rpm, 2 h, 45°C	20 s-5 min, 40-70%	185 – 368	0.17 – 0.54
SO (1-30%) / SL (1.2%)	15,000 rpm, 10 min, 30°C	4 min, 25%	144 – 455	0.20 – 0.27
SO (20-80%) / RH (20-80%)	275 rpm, 2 h, 45°C	N/A	25 – 734	0.06 – 0.65
SO (5-20%) / Tween80 (1%)	15,000 rpm, 10 min, 30°C	2-4 min, 25%	198 – 724	0.17 – 0.29
SO (20%) / TW (1%)	10,000 rpm, 10 min, 30°C	1-8 min, 20%	353 – 472	0.01 – 0.27
SO (50%) / TW (0.25%)	10,000 rpm, 10 min, 30°C	4-8 min, 20%	1384 – 1473	0.05 – 0.43
SO (20-30%) / HS (20-30%)	15,000 rpm, 5 min, 30°C	4 min, 25%	91 – 175	0.02 – 0.40
MCM (0.25-20%) / F68 (2%)	275 rpm, 2 h, 45°C	80 s, 40%	129 – 337	0.27 – 0.58
MCM (0.25-20%) / EL (1%)	275 rpm, 2 h, 45°C	80 s, 40%	93 – 614	0.19 – 0.51
MCM (0.25-20%) / RH (1%)	275 rpm, 2 h, 45°C	80 s, 40%	61 – 511	0.25 – 0.58
WL (0.25-20%) / SL (1.2%)	15,000 rpm, 10 min, 30°C	3-4 min, 25-40%	88 – 390	0.11 – 0.38
WL (2.5-20%) / RH (10%)	275 rpm, 2 h, 45°C	N/A	73 – 603	0.25 – 0.92
WL (1.25-20%) / HS (10%)	275 rpm, 0.5 h, 45°C	5 min, 40%	82 – 504	0.13 – 0.52
WL (20-50%) / HS (0.25-10%)	5,000-20,000 rpm, 2-10 min, 30°C	2-6 min, 20%	175 – 1368	0.03 – 0.22

SO: Soybean oil; SL: Soybean lecithin; RH: Kolliphor® RH40; TW: Tween® 80; HS: Kolliphor® HS15; MCM: Capmul® MCM NF; F68: Pluronic F68; EL: Kolliphor® EL; WL: LabrafacTM lipophile WL1349. N/A: Not applicable; PI: Polydispersity Index. Droplet size and PI were determined at 100-fold dilution.

Table 2.2 Commercial name, chemical structure and HLB of the selected ingredients

Commercial name	Chemical structure	Description
Capmul® MCM NF	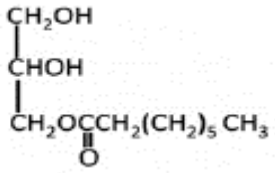	Glyceryl caprylate/caprate; Medium chain C8-, C10- monoglyceride; HLB= 5-6
Labrafac™ Lipophile WL1349	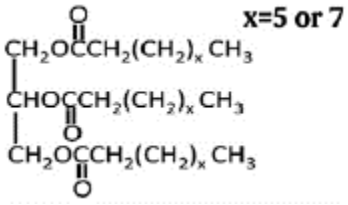	Glyceryl tricaprylate/tricaprate; Medium chain C8-, C10- triglyceride; HLB=1
Kolliphor® HS15	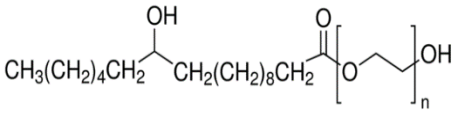	Polyoxyl 15 hydroxystearate; Polyglycol mono- and di-esters of 12-hydroxystearic acid and of about 30% of free polyethylene glycol; HLB = 14-16

HLB = Hydrophile-lipophile balance

Table 2.3 Summary of the NE formulation and sonication specifications

	Formulation				Sonication specifications	
	MCM (mg)	**WL (mg)**	**HS (mg)**	**H_2O (q.s., mg)**	**Amplitude (%)**	**On-duty time (min)**
SE	250	250	500	5000	N/A	N/A
ME	N/A	1200	300	3000	20	6
LE	N/A	1200	15	3000	20	6

N/A = Not applied, MCM = Capmul® MCM NF, WL = Labrafac™ Lipophile WL1349, HS = Kolliphor® HS15, SE = Small-sized NE, ME = Medium-sized NE, LE = Large-sized NE

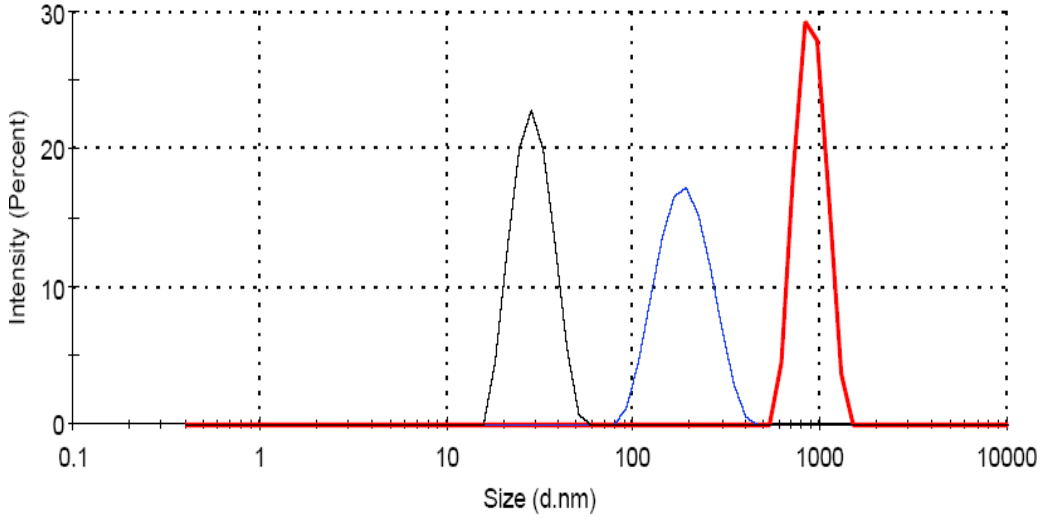

Figure 2.2 Droplet size distribution of SE, ME and LE. The droplet sizes were determined for SE (grey, 30 ± 9 nm), ME (blue, 212 ± 64 nm) and LE (red, 893 ± 158 nm) by dynamic light scattering at 100-fold dilution in distilled water to prevent multiple scattering. The peaks were distinct to each other without overlapping to ensure proper interpretation of *in vivo* results. Data were presented as the size distribution for one experimental.

Table 2.4 SE, ME and LE mean droplet size and PI determined by DLS (Mean ± SD, n=3)

	Droplet size (nm)	PI
SE	29 ± 1	0.06 ± 0.02
ME	214 ± 2	0.11 ± 0.02
LE	883 ± 16	0.11 ± 0.10

2.3. The stability tests for the NEs

2.3.1. Materials and methodology

The prepared NEs were subjected to the stability tests including stability during storage under ambient temperature, stability against serial dilutions and stability in mice plasma *in vitro*.

For the stability at ambient temperature, the prepared NEs were sampled for DLS droplet size determinations at 100-fold dilution in distilled water every 24 h for 3 days. The droplet size of SE and ME was also measured at 3 months while LE was visually observed every day after 3 days until phase separation occurred. For the stability against dilutions, the NEs were diluted 5-1000 folds in pH 7.4 phosphate buffer saline (PBS) prior to droplet size determination by DLS. For the stability in mice plasma, 100 µL NEs (without dilution) was incubated with 100 µL mice plasma (Rockland antibodies and assays, Pennsylvania) at 100 rpm, 37°C. At sampling time point, a 40 µL aliquot was sampled and diluted 50-fold in PBS prior to droplet size determination by DLS.

2.3.2. Results and discussions

2.3.2.1. NEs stability under ambient temperature

Figure 2.3 shows the droplet size change upon storage time at ambient temperature. Within 3 days, no significant droplet size changes were observed for all NEs. Notably, the droplet size variation for LE started to increase as early as Day 2. Since NE by nature is kinetically stable but thermodynamically unstable system (Gupta et al., 2016), the low concentration of HS in LE resulted in a faster droplet aggregation which eventually led to the phase separation on Day 7. SE and ME on the other hand, were much more stable up to the last observation time at 3 months. Apparently, the ultrasonication played a critical role to stabilize the NEs especially LE which

otherwise separated in less than 15 min without this process. Though LE had limited thermodynamic stability, a 72-h stable system was sufficient for the purpose of the current study.

2.3.2.2. NEs stability against dilutions

Figure 2.4 illustrates the impact of dilutions on the NEs. SE presented a good stability with no droplet size changes at all the tested dilution levels (5- to 1000-fold dilution) with the average size ranging from 24 nm to 32 nm. ME demonstrated size variation at 5-fold dilution (110 ± 14 nm) and 10-fold dilution (155 ± 9 nm). Further dilution of ME from 50- to 1000-fold did not cause significant change in size with the mean droplet size ranging from 187 nm to 219 nm. The variations at lower dilution for ME and LE were likely due to the multiple scattering phenomenon by DLS since they both had much higher lipid concentrations versus SE. Multiple scattering refers to the phenomenon wherein photons scattered from the analyte are re-scattered from neighboring particles prior to reaching the instrument detector (Malvern technical bulletin). Therefore, this phenomenon occurs at higher particle concentration. The net result then, is that DLS size measurements in the presence of multiple scattering will be biased toward smaller sizes.

LE showed variations in size upon dilution. Besides the size changes at lower dilution level (764 ± 310 nm at 5-fold and 1249 ± 198 nm at 10-fold), the droplet size also showed significant increase to 1782 ± 542 nm at 1000-fold dilution. This was probably because at this dilution level, the relative concentration of HS was not enough to reduce the surface tension, which resulted in the aggregation of the droplets. However, the LE droplet size appeared to be stable upon dilutions from 20 to 500-fold. And the estimated dilution of the NE after i.v. injection is in this range. Therefore, the stability of size at this range of dilution assures the LE size will not change due to dilution by plasma in the *in vivo* studies.

2.3.2.3. NEs stability in mice plasma *in vitro*

As depicted in **Figure 2.5**, when incubated at 37 °C under mild shaking condition, ME and LE did not show droplet size change for 4 h which could be attributed to the use of Kolliphor® HS15 (HS). HS is a PEGylated surfactant which comprises of 15 units of PEG monomer as the hydrophilic head. Due to the high hydrophilicity, chain flexibility, electrical neutrality, PEG helps to sterically stabilize NPs and prevent the interactions with biological components (Gref et al., 1995; Avgoustakis, et al., 2003). Contrarily, SE droplet size increased from 1 h and became comparable to that of ME after 4 h despite the use of HS. This could be due to the much smaller size hence significantly larger surface area. The enhanced surface area might facilitate the interactions between the droplets and plasma protein.

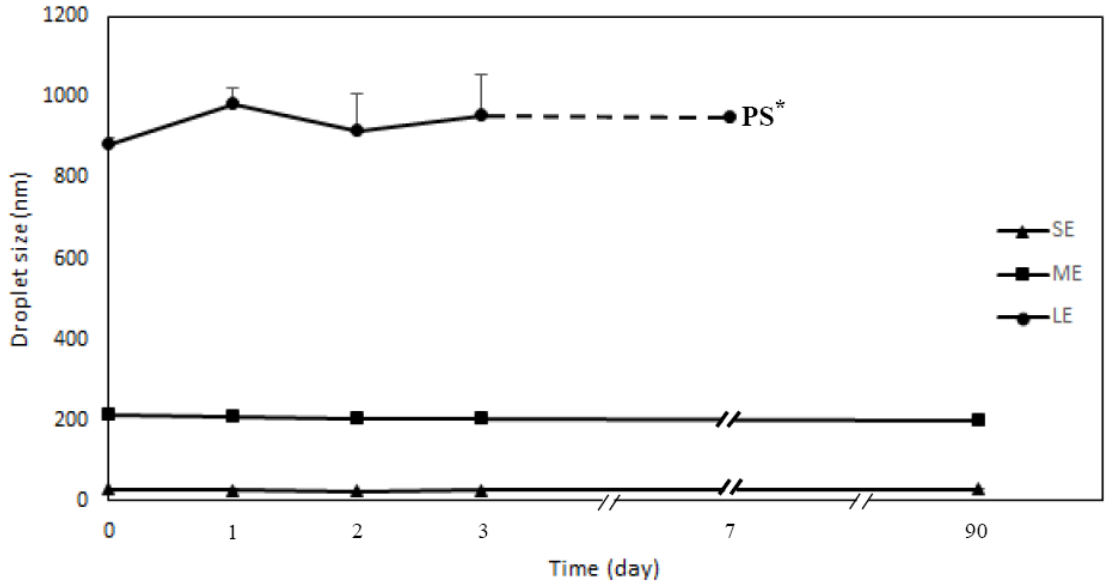

Figure 2.3 The NEs stability under ambient temperature. At sampling time points, the NEs were sampled and diluted 100-fold in distilled water prior to droplet size determination by DLS. There was no droplet size change over 3 days for all three NEs. However, phase separation (*) was observed for LE after 7 days post preparation. SE and ME did not show droplet size change until 90 days (Mean ± SD, n=3).

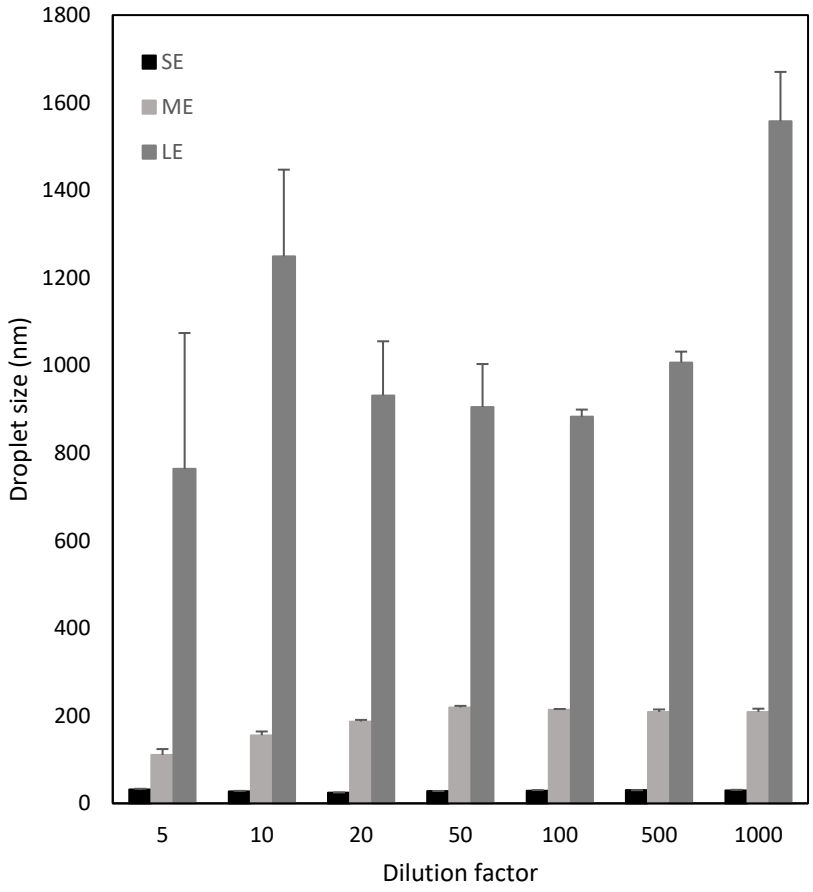

Figure 2.4 NEs stability against dilutions in pH 7.4 PBS. Freshly prepared NEs were subject to different folds of dilutions in pH 7.4 PBS and the droplet sizes was determined by DLS (Mean ± SD, n=3).

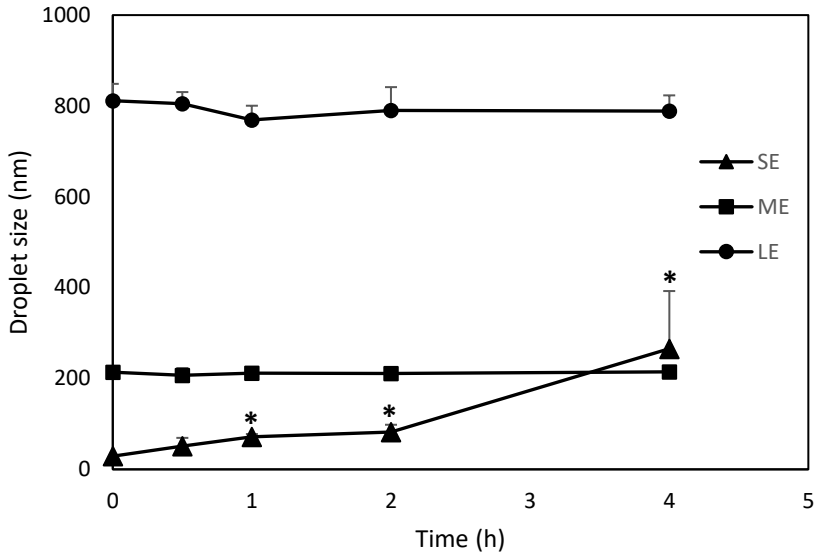

Figure 2.5 NEs stability in mice plasma *in vitro*. NE were incubated with mice plasma at 37°C, 100 RPM *in vitro*. The droplet size was measured by DLS after 100-fold dilution in PBS (Mean ± SD, n=3). *: Significantly different from the droplet size at time 0, $P < 0.05$.

2.4. Summary

The NEs with distinct droplet sizes, i.e., the small-size NE (SE) of ~30 nm, the medium-size NE (ME) of ~200 nm and the large-size NE (LE) of ~ 900 nm, respectively, were successfully prepared. Unlike the NEs in the literature, these NEs, especially LE, demonstrated a narrow and well-defined droplet size distribution. The corresponding peaks of the three NEs did not overlap with each other so that they would not cause interference for the *in vivo* assessment. The NEs were subject to various stability tests. The results suggested that all the NEs demonstrated stability for at least 3 days when stored under ambient temperature. In addition, they were also stable against 20- to 500-fold dilution in pH 7.4 PBS. When incubated with the mice plasma *in vitro*, SE droplets tended to increase after 1 h whilst ME and LE maintained the initial droplet size.

Chapter 3. Establishment of DiI fluorometry and biological sample preparation protocol

In this chapter, the following topics are addressed:

- The development and validation of the fluorometry for DiI
- The establishment of the *in vivo* animal model
- The establishment of the preparation protocol and assay for biological samples

3.1. Introduction

Fluorescence dyes have found use in a wide spectrum of geological, biological and pharmaceutical sciences. Compared to fluorescent proteins, they present smaller molecules, better photostability and brightness, and the absence of maturation time (Süel et al., 2011). The fluorescence marker technology can be used to determine a variety of substances such as environmental pollutants, drugs, amino acids and nucleotides (Suzuki et al., 2015). The use of the fluorescent dyes extends to immunofluorescence microscopy, flow cytometry, cellular staining, tracking and intra-/inter-cellular trafficking, etc. In the field of nanotechnology, fluorescent dyes have also seen extensive applications in the evaluations of *in vivo* biological fate of different types of NPs such as polymeric NPs (Reisch et al., 2016), micelles (Wei, 2019) and liposomes (Tansi et al., 2015), etc.

The capabilities of a fluorescent dye used in the biological studies are mainly dependent on its physical properties. The extinction coefficient (the extent to which a fluorophore absorbs light), the quantum yield (the emission of fluorescence from an excited fluorophore) and the photostability are among the most important considerations when selecting the dyes (Wells et al., 1990). Some commonly used dyes in pharmaceutical research include fluorescein isothiocyanate (FITC), rhodamines and lucifer yellow (LY), etc., each with advantages and limitations (Brelie, 1993). For example, FITC provides reasonably large extinction coefficient and high quantum yields after conjugation with biological molecules, however it also associates with unfavorable properties such as aqueous decomposition, limited photostability, pH-sensitivity and overlapping emission spectrum with autofluorescence. Rhodamine, on the other hand, though more photostable and pH-insensitive, poses significantly lower quantum yield thus much dimmer fluorescent signals. Similarly, LY presents intense fluorescence and reasonable photostability whilst the extremely broad excitation and emission spectra complicate its detection in the presence of other fluorophores.

Besides the above fluorescent dyes, the group of carbocyanine dyes (cyanines) has been developed and remained as the most prevalent fluorophores for *in vivo* imaging due to the long excitation and emission wavelengths which are distinguished from most of the autofluorescence generated by endogenous fluorophores from the body (Croce et al., 2014). Among the cyanine family, DiI (1,1'-dioctadecyl-3,3,3',3'-tetramethylindocarbocyanine perchlorate, **Figure 3.1**), also known as DiIC18(3), provides some features such as (1) It diffuses laterally within the entire cell and subsequently well retained with little transfer to other cells; (2) It is weakly fluorescent in water but highly fluorescent and photostable in lipid membrane; (3) It possesses very bright signals with high extinction coefficients (Invitrogen, 2010); (4) It does not appreciably affect cell viability, development, or basic physiological properties (Honig and Hume, 1989). Due to these

properties, DiI has been used in cellular staining (Fallatah et al., 2019), *in vivo* cell tracing (Endepols, 2001), ligand-receptor molecular transfer (Xu, 1992), etc. In addition, the water insolubility of DiI potentially render its usefulness especially in labeling lipid-based drug delivery system (LBDDS) such as NE. All these properties make DiI a good labeling candidate for the current study. To the best of our knowledge, DiI has not yet been utilized as a quantitative labeling agent for DDS. Therefore, it is important to establish DiI quantitative fluorometry method and to evaluate its suitability for the *in vivo* study purpose.

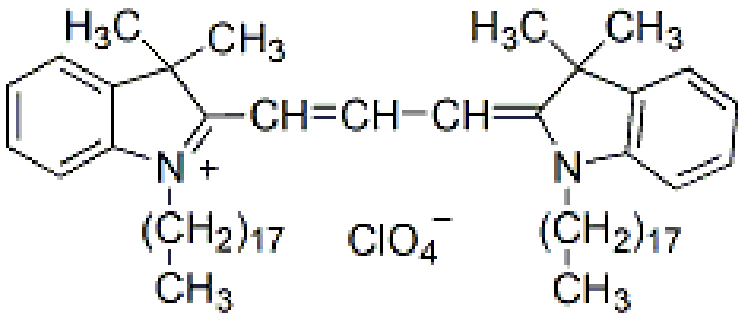

Figure 3.1 Chemical structure of DiI

3.2. DiI fluorometry method establishment and validation

3.2.1. Materials and methodology

DiI was purchased from Biotium (Biotium Inc., CA). Dimethylsulfoxide (DMSO) was of reagent grade (BDH, VWR). DiI Stock Solution (400 µg/mL) was prepared by the dissolution of DiI crystals in DMSO. The Standard Working Solutions were subsequently prepared from the Stock Solution to produce a DiI concentration range from 1.0 to 1000 ng/mL. Two hundred µL of the Standard Working Solutions was added to a well of 96-well black microplate and the fluorescence intensity was measured by a Glomax® Fluorescence Microplate Reader (San Luis Obispo, CA, USA) with the high sensitivity mode at room temperature. The excitation and emission wavelengths were 520 nm and 580-640 nm, respectively. The experiment was conducted in triplicate. The fluorescence intensity was plotted versus the DiI concentrations to obtain the standard calibration curve. The assay method was validated by accuracy and intermediate precision. Briefly, the accuracy of the method was conducted by the determination of a set of DiI solutions with known concentrations (5, 20, 50, 200 and 500 ng/mL). The measured concentration was compared to the theoretical concentration to obtain the percentage recovery. Intermediate precision was evaluated on different days to determine the relative standard deviation (%RSD).

3.2.2. Results and discussions

Figure 3.2 shows the linear regression curve for DiI standard solutions. The assay method had a linear range of 1.0 to 1000 ng/mL with a correlation coefficient of 0.9998 indicating a good correlation between DiI concentration in DMSO and its corresponding fluorescence intensity. The percentage recovery for the accuracy test of five known concentration standards (5, 20, 50, 200

and 500 ng/mL) was found to be 95.7 ± 4.2% (**Table 3.1**). In addition, the intermediate precision results indicated a 1.7% to 2.7% RSD (**Table 3.2**) throughout the concentrations within the linear range. The data demonstrated that the established fluorometry method for DiI was valid and reproducible. Furthermore, the lowest DiI concentration of 1.0 ng/mL which exhibited three times signal-noise ratio was comparable to that of Rhodamine-B of 0.5 ng/mL (Huang et al., 2016) and FITC of 2.2 ng/mL (Imasaka et al., 1977). This high sensitivity rendered practical use for the analysis of *in vivo* biological samples in which compounds of interest are usually presented in the concentration range of μg/mL, though the interference from the sample matrix should be carefully evaluated.

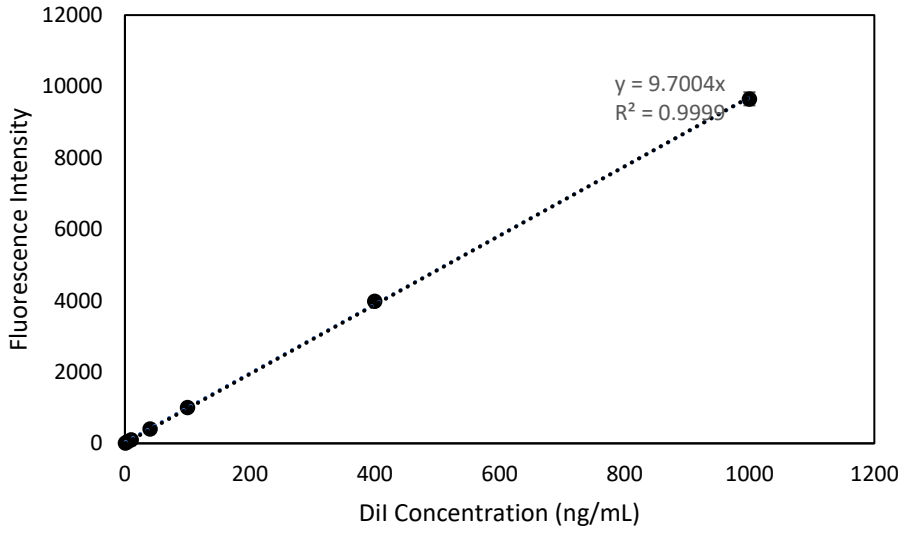

Figure 3.2 DiI standard calibration curve in DMSO (Mean ± SD, n=3).

Table 3.1 Accuracy of DiI fluorometry method (Mean ± SD, n=3)

Nominal Concn. (ng/mL)	Calculated Concn. (ng/mL)	Recovery (%)
5	5.1 ± 0.1	101.8 ± 1.8
20	19.2 ± 0.6	96.0 ± 2.8
50	48.0 ± 0.3	96.1 ± 0.6
200	188.3 ± 1.3	94.2 ± 0.6
500	451.2 ± 9.6	90.2 ± 1.9
MEAN ± SD (n=5)		**95.7 ± 4.2**

Table 3.2 Intermediate precision of DiI fluorometry method (n=3)

DiI Concn. (ng/mL)	RSD (%)
1	2.7
4	2.3
10	1.7
40	1.7
100	1.9
400	1.7
1000	1.9

3.3. The characterizations of DiI

3.3.1. Materials and methodology

Mice plasma (directly from non-hemolyzed blood from healthy and fasted donor) was purchased from Rockland Immunochemicals, Inc. (Pottstown, PA, USA) The stability of DiI in mice plasma was evaluated by incubation of 100 µL of DiI Standard Solution in Ethyl Alcohol (40 µg/mL) with 1.9 mL mouse plasma. The mixture was vortexed for 10 s and 10 µL aliquot was immediately assayed to determine the DiI concentration at time 0. The plasma was then shaken at 200 rpm under 37°C in the dark. At each sampling time point (0.25, 0.5, 1 and 2 h), 10 µL aliquot was diluted in DMSO prior to the fluorescence intensity measurement. DiI concentration at each time point was presented as the percentage versus the concentration at time 0.

The solubility of DiI in WL was determined by the addition of an excessive amount of DiI in WL. The mixture was shaken at 25°C for 72 hours. The mixture was subsequently centrifuged at 15,700 g for 5 min and the supernatant was properly diluted in DMSO prior to the fluorometric assay.

The partition coefficient of DiI in WL and MCM versus water was evaluated. Briefly, one mg of DiI was dissolved in 5 g of the lipids, respectively. Subsequently, equivalent volume of deionized water was added, and the mixture was shaken at 37°C, 200 rpm for 24 hours. The mixture was transferred to a separatory funnel to equilibrate and separate the two phases and each phase was assayed for DiI after proper dilution in DMSO. The Log partition coefficient was calculated based on the DiI concentration in each phase.

The above experiments were conducted in triplicate.

DiI loaded NEs were prepared according to the formulations and subsequent preparation procedures described in **Section 2.1.1.**, except for that DiI was first dissolved in WL to achieve a concentration of 2.5 mg DiI/g WL. The droplet size of DiI labeled NEs were measured by DLS at 100-fold dilution in pH 7.4 PBS.

3.3.2. Results and discussions

Figure 3.3 depicts the stability of DiI in mice plasma. There was no degradation of DiI in 2 h indicating its photostability in mice plasma. In addition, DiI was characterized for lipophilicity. DiI had a 5.51 ± 0.09 mg/g WL solubility. **Figure 3.4** illustrates DiI partition coefficient between WL/MCM and water. The high lipophilicity of DiI (log P = 4.31 ± 0.03, n=3) in WL versus water ensured the complete encapsulation of the dye in the NE droplets. These findings together suggested that DiI was a suitable fluorescent dye to label NEs. Finally, DiI was loaded into the NEs. **Figure 3.5** shows the visual appearance of the DiI loaded SE (DSE), DiI loaded ME (DME) and DiI loaded LE (DLE), respectively. **Table 3.3** summarizes the droplet size of DiI loaded NEs. The NEs droplet size was not affected by the loading of DiI. DSE had a final DiI concentration of 0.2 mg/mL, whilst DME and DLE 1 mg/mL, respectively.

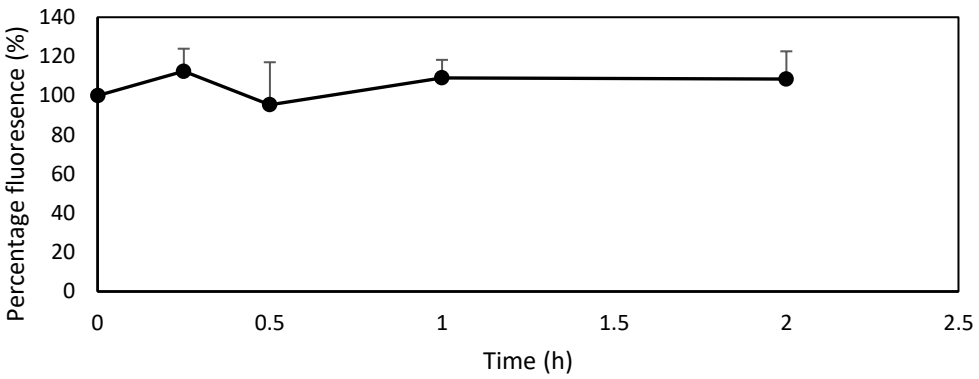

Figure 3.3 DiI stability in mice plasma. DiI was incubated with mice plasma at 37°C for 2 h in dark (Mean ± SD, n=3).

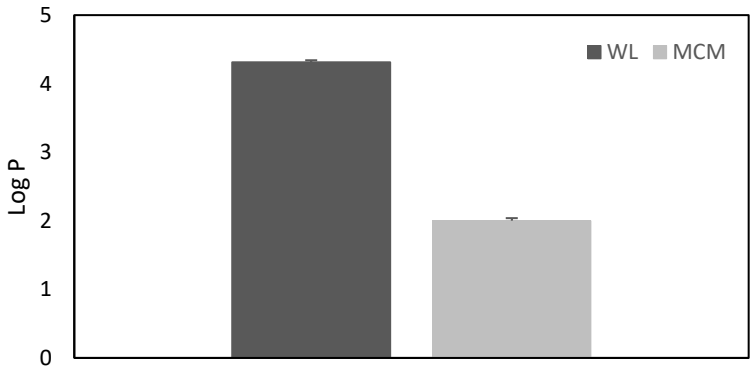

Figure 3.4 Partition coefficient of DiI in WL and MCM versus water (Mean ± SD, n=3).

Figure 3.5 Photos of DiI-loaded NEs. DiI loaded SE (DSE, 0.2 mg/mL) had a transparent appearance whilst DiI loaded ME (DME, 1 mg/mL) and LE (DLE, 1 mg/mL) were milky.

Table 3.3 DSE, DME and DLE mean droplet size and PI determined by DLS (Mean ± SD, n=3)

	Droplet size (nm)	PI
SE	29 ± 2	0.06 ± 0.01
ME	197 ± 3	0.16 ± 0.02
LE	843 ± 101	0.34 ± 0.13

3.4. Tumor-bearing mice model

3.4.1. Cell culture

RPMI 1640 medium with L-glutamine, Hanks' balance salt solution (HBSS), MEM vitamin, sodium pyruvate were purchased from Hyclone (Hyclone, UT). Fetal bovine serum (MilliporeSigma, MA), non-essential amino acids (Sigma Aldrich, MO), trypsin/EDTA (ATCC, VA), trypan blue (Nano Entek, South Korea), cell strainer (40 μm, Greiner Bio-One, Austria) were purchased through VWR. The complete medium (CM) was prepared under sterile condition according to **Table 3.4** (Overwijk and Restifo, 2001)

B16F10 melanoma cell was purchased from the National Cancer Institute (NCI). Upon arrival, the cell was rapidly thawed in 37°C water bath for 1.5 min until movement of ice clump occurred. The cell suspension was diluted in CM and centrifuged at 660 g for 10 min at 4°C (Eppendorf 5804R, Germany). The cell pellet was resuspended in 3 mL CM which yielded 7.36×10^{5} mL^{-1} with 92% viability determined by trypan blue staining using a hemocytometer (Countess II FL, Life Technologies, CA). The cells were subcultured in CM at 37°C with 5% CO_2 and were split at 1:10 to 1:5 ratio when 50% confluent. Cells with more than 95% viability were cryopreserved in 90% CM and 10% DMSO and stored in nitrogen vapor for future use.

3.4.2. Mice inoculation

Female C57BL/6J mice of 8-week old were purchased from Taconic Biosciences (Germantown, NY) and housed at the Animal Care Center at St. John's University. The mice inoculation procedures were according to the protocol established by the NCI. (Overwijk and Restifo, 2001) Briefly, B16F10 melanoma cells were harvested by trypsin/EDTA at less than 50% confluence to

ensure the cells under logarithmic growth phase. Cells were resuspended in ice-cold HBSS and passed through disposable cell strainer to remove clumps. The final concentration was adjusted to 1×10^6 cell/mL with a viability > 90%. The cell suspension 100 µL was injected subcutaneously (10^5 cells/mouse) into the right flank of the mice. The tumor size was measured every day after 7 days by a caliper and calculated by **Eq. (1)**:

$$\text{Tumor size} = ½ \times L \times W^2 \qquad \textbf{Eq. (1)}$$

Where L was the length and W was the width of the tumor. (Tomayko and Reynolds, 1989)

When the tumor volume reached 120 mm^3 or any dimension of the tumor measured 18 mm, the further experiments were then carried out.

Table 3.4 The complete medium for B16F10 melanoma

Medium	Final concentration	Volume (mL)
RPMI1640 w/ L-glutamine	-	500
Fetal bovine serum (FBS)	10% v/v	55
Non-essential amino acids (100×)	100 μM	5.5
Sodium pyruvate (100 mM)	1 mM	5.5
MEM vitamin (100×)	-	7.5

3.5. Biological sample preparation and DiI extraction protocol

3.5.1. Materials and methodology

Subcutaneous B16F10 melanoma bearing female C57BL/6J mice were anesthetized by 2.5% isoflurane inhalation. The blood was collected by cardiac puncture and then centrifuged at 2,000 g, 4°C for 10 min to obtain the plasma. The mice were then sacrificed by carbon dioxide asphyxiation. The major organs including the heart, liver, spleen, lungs, kidneys, stomach, small intestine, colon, brain and tumor were collected. The tissues were wiped, weighed and homogenized by Pyrex® Tenbroeck homogenizer (Corning, NY) in deionized water at 1:4 or 1:9 (w/v). The tissue homogenate and plasma were spiked with DiI standard solution by a HPLC manual syringe (ThermoFisher Scientific, Waltham, MA) at 0.1, 1, 10 and 50 $\mu g*g^{-1}$ (DiI/tissue), respectively. Non-spiked tissue homogenates were used as the blank references. The spiked homogenates were extracted by two protocols. In the first protocol, equivalent volume of Ethyl Acetate (EA) was added to the homogenate, and the mixture were vortexed at 2,000 rpm for 30 min (Scientific Industries, NY) followed by centrifugation at 15,700 g for 5 min. The supernatant was diluted in DMSO and subjected to the fluorometry method. In the second protocol, equivalent volume of EA was added to the homogenate, and the mixture was vortexed at 2,000 rpm for 10 min followed by centrifugation at 15,700 g for 5 min. The supernatant was collected and replaced by equivalent volume of EA. The mixture was vortexed again at 2,000 rpm for 10 min and centrifuged with the same condition to obtain the second supernatant. Both aliquots of the supernatant were diluted respectively in DMSO prior to fluorescence measurement. The extraction efficiency was presented as the percentage recovery of DiI. The experiments for the two protocols were individually conducted for at least three times. One-way analysis of variance (ANOVA) and two-tail paired t-test were conducted and a $P < 0.05$ was considered as significantly different.

3.5.2. Results and discussions

The mice were inoculated with 10^5 B16F10 melanoma subcutaneously. Tumor became visible usually after 7 days and reached 120 mm^3 in 10 to 14 days. To evaluate the extraction efficiency of DiI from various biological samples, we investigated two extraction protocols. The first protocol involved a single extraction on the spiked or blank tissues for 30 min (**Figure 3.6**) whilst the second protocol utilized a double extraction each for 10 min (**Figure 3.7**). Despite the longer total vortex time in the single extraction method, DiI recovery from all the biological samples fell in the range from 60 to 75% with the RSD ranging mainly from 10.9% to 24.9%. Nevertheless, when the double extraction was applied, though the total vortex time was shortened, DiI recovery were found mainly above 80% and for certain tissues over 90% with the RSD ranging mainly from 3.2% to 11.3%. This contrast suggested the double extraction protocol was capable of extracting DiI more efficiently and precisely from the various biological samples.

Due to the complexity of *in vivo* biological sample matrix and the autofluorescence from various endogenous fluorophore (Croce and Bottiroli, 2014), it was important to evaluate and eliminate such interferences. The blank tissues therefore served for this purpose and underwent the same extraction protocols. The results showed that the EA extracts showed similar signal as the blank solvent reading which suggested the good specificity of the extraction protocols and the developed fluorometry.

Statistical analysis was performed for the double extraction method to investigate whether there were differences among concentration levels for a given tissue and if there were differences among tissues within a given concentration level. The results demonstrated there was no significant difference in the mean extraction ratio of any given tissue among the concentration groups (0.1, 1, 10 and 50 µg/g tissue). This indicated the extraction method was consistent and reliable to extract DiI at least within the tested concentration range. However, various tissue

spiked with the same concentration of DiI exhibited different mean extraction ratio from 70.2% to 97.0%. Such difference could be due to the difference of the lipophilic compositions in the tissue. For example, glial cells and lipophilic endocannabinoids are mostly abundant in the central nervous system (Scheller and Kirchhoff, 2016). In contrast, the stomach is uniquely comprised of three layers of highly content of smooth muscle. Due to such tissue variance, the grand mean (n=12) of the extraction ratio from a certain tissue was determined and would be further used individually as shown in **Table 3.5**.

Table 3.5 DiI extraction efficiency from biological tissues (Mean ± SD, n=12)

Tissue	Extraction efficiency (%)
Heart	79.5 ± 3.0
Liver	76.8 ± 1.2
Spleen	82.6 ± 4.1
Lungs	83.0 ± 2.6
Kidneys	87.0 ± 2.5
Stomach	74.6 ± 3.2
Small Intestine	80.2 ± 2.4
Colon	78.5 ± 2.0
Brain	93.4 ± 1.0
Tumor	84.3 ± 4.2
Plasma	90.1 ± 2.9

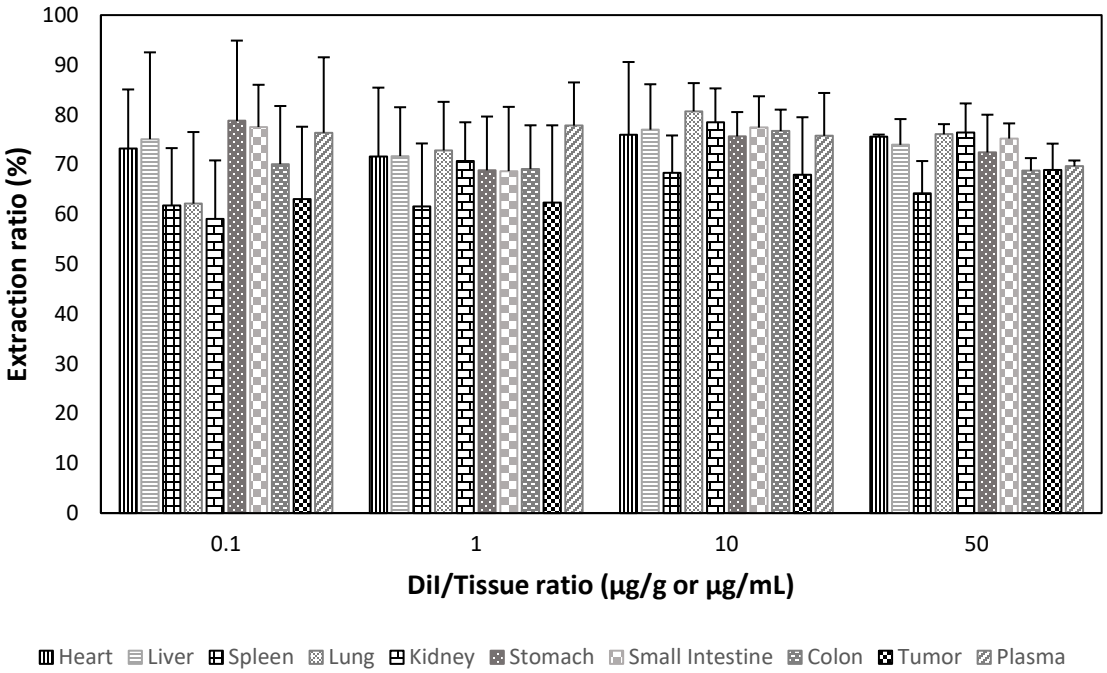

Figure 3.6 Biological sample DiI extraction ratio by the single extraction protocol (Mean ± SD, n=6).

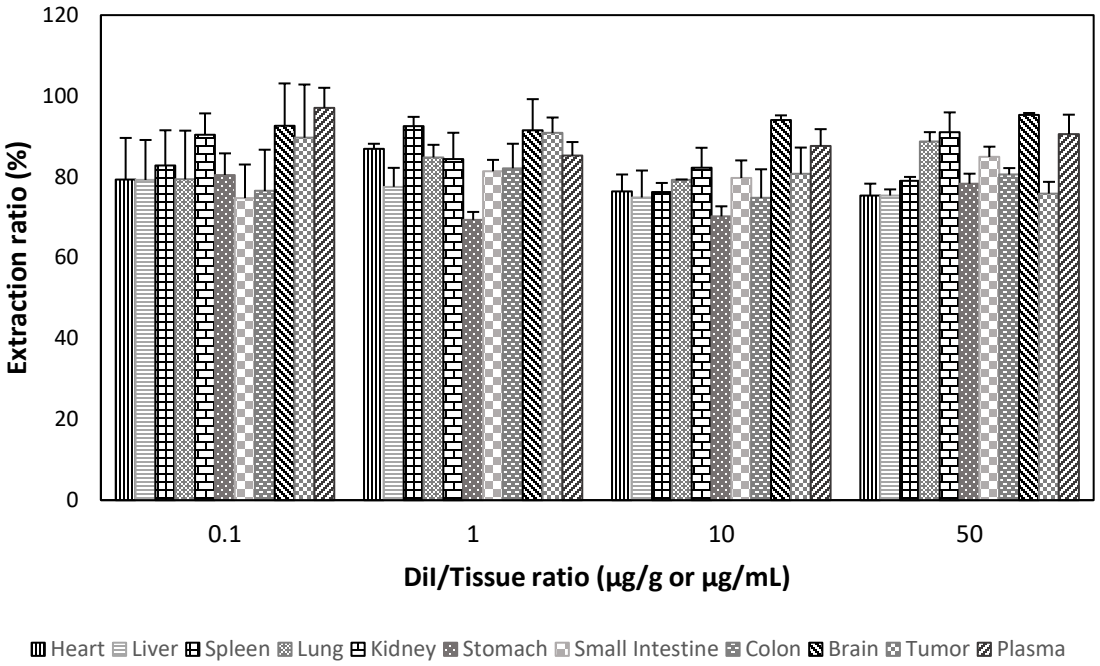

Figure 3.7 Biological sample DiI extraction ratio by the double extraction protocol (Mean ± SD, n=3). There was no significant difference of the extraction ratio from a given tissue among concentration groups. However, tissues within the same concentration group exhibited different mean extraction ratios.

3.6. Summary

A fluorometry method for DiI was established and validated for accuracy and intermediate precision. DiI demonstrated high sensitivity with a linear range of 1.0 to 1000 ng/mL. DiI was characterized for its lipophilicity, with a log P of 4.31 and 2.00 in WL/H_2O and MCM/H_2O system, respectively. The stability of DiI in mice plasma was investigated *in vitro* and found to be stable for the 2-h experimental period. In addition, DiI-loaded NEs were prepared, which showed same droplet size and stability as the blank NEs. Furthermore, B16F10 melanoma bearing C57BL/6J mice model was established. Finally, the biological sample preparation and DiI extraction protocol were developed and evaluated. DiI extraction ratio from various tissues was determined to be 79.5% for the heart, 76.8% for the liver, 82.6% for the spleen, 83.0% for the lungs, 87.0% for the kidneys, 74.6% for the stomach, 80.2% for the small intestine, 78.5% for the colon, 93.4% for the brain, 84.3% for the tumor and 90.1% for the plasma.

Chapter 4. The *in vivo* biodistribution of the DiI-loaded nanoemulsions

In this chapter, the following topics are elaborated:

- The *in vivo* biodistribution experimental procedure and bioassay
- DiI concentration-time profiles in various tissues after intravenous injection of DiI solution (DS), DSE, DME and DLE
- The interpretation of the biodistribution data and the evaluation of NE size-dependent biodistribution

4.1. Materials and methodology

Female C57BL/6J mice of 8-week old were purchased from Taconic Biosciences (Germantown, NY) and housed at the Animal Care Center at St. John's University. The mice were inoculated with B16F10 melanoma subcutaneously according to **Section. 3.4.2.** When the tumor volume reached 120 mm^3 or any dimension of the tumor measured 18 mm (usually in 10 to 14 days), the following experiments were carried out. The mice were randomly and evenly divided into 4 groups (21 mice/group). The mice were restrained in a mice restrainer, and then injected through the tail vein with DiI solution in 19% ethanol (DS), DSE, DME and DLE at the DiI dose of 5, 2, 5 and 5 mg/kg, respectively. Sterile dextrose for injection (5%) (D5W, Baxter, IL) was used as the diluent in the formulations instead of distilled water. DSE was given at a lower dose due to its higher viscosity not suitable for direct intravenous administration thus a dilution was performed.

At each sampling time point (0.25, 0.5, 1, 2, 4, 6 and 10 h) post injection, three mice from each group were anesthetized with 2.5% isoflurane inhalation. The blood was collected by cardiac puncture and centrifuged at 2,000 g, 4 °C for 10 min to obtain the plasma (P). The mice were then immediately euthanized by carbon dioxide asphyxiation. The major organs including heart (H), liver (V), spleen (S), lungs (L), kidneys (K), stomach (T), small intestine (I), colon (C), brain (B) and tumor (U) were collected and all the biological samples were stored under -20 °C until analysis.

DiI concentration in the biological samples was determined by the established protocol (See **Section 3.5.**). Briefly, the organs were weighed and homogenized with deionized water at 1:4, w/v. Two hundred and fifty μL of the homogenized sample was mixed with equivalent volume of EA and vortexed for 10 min at 2000 rpm followed by centrifuge at 15,700 g for 5 min. The supernatant was collected and replaced by equivalent volume of fresh EA. The mixture was vortexed for another 10 min at 2,000 rpm and a subsequent 5-min centrifuge at 15,700 g to obtain the second supernatant. Both aliquots of the supernatant were then diluted in DMSO and subject to the fluorometry method. DiI concentration in tissues was determined by the corresponding tissue extraction ratio (See **Table 3.5**) and the concentration-time profile was plotted.

The major pharmacokinetics (PK) parameters were calculated by Phoenix® WinNonlin® (Certara, NJ). One-way analysis of variance (ANOVA) and two-tail paired t-test were conducted where applicable and a $p < 0.05$ was considered as significantly different.

4.2. DiI concentration-time profiles in tissues

Figure 4.1 through **Figure 4.4** depict the DiI concentration-time profiles in various tissues followed by the administration of DS, DSE, DME and DLE, respectively. The comparison and

discussions in the following sections will be mainly focused on the observed concentrations and the apparent maximum concentrations (C_{max}). Lists of the calculated PK parameters such as area under the curve (AUC), mean residence time (MRT) and detailed discussions, can be found in the **Appendix**.

4.2.1. DiI tissue concentration-time profiles after i.v. administration of DS

As a lipophilic compound with small molecular weight, DiI showed a rapid concentration decline in the plasma when given in the solution form (**Figure 4.1**). After 2 h, it was completely cleared from the plasma. Such fast plasma clearance could be partially due to the rapid tissue distribution, evidenced by the higher than plasma concentration in the liver, spleen and lungs at as early as the first sampling time point (0.25 h). It could also be possibly due to the partial precipitation of DiI upon instant dilution in the plasma. DiI concentrations in these tissues all peaked within 0.5 h with apparent C_{max} of 16.34, 32.68 and 15.52 μg/g in the liver, spleen and lungs, respectively. In addition, a remaining DiI concentration was observed within these tissues in the late stage which could be due to the portion uptaken by the tissues and this process could be implemented by the two 18-carbon chains which firmly anchor in the cell membrane (Honig and Hume, 1986). On the other hand, it was observed that the distribution of DiI in heart, kidney, stomach, small intestine, colon and tumor was much less than that in liver, spleen and lung, with the apparent C_{max} in these tissues ranging from 0.23–2.74 $\mu g*g^{-1}$.

4.2.2. DiI tissue concentration-time profiles after i.v. administration of DSE

When DSE was administered intravenously to the mice, DiI plasma concentration dropped quickly but maintained, though low, at a constant level throughout the experiment period (**Figure**

4.2). Such "sustaining" effect was also seen in the various tissues: DiI concentrations showed more or less stable levels up to 10 h despite their peak concentrations occurred almost all early at 0.25 h. In certain tissues such as the liver, spleen, stomach, colon and tumor, the DiI concentration at last sampling point (10 h) was higher than the previous one, indicating that the terminal elimination phase had not been reached at the end of the experiment (10 h). In addition, the apparent C_{max} in liver and spleen was 1.44 and 1.13 $\mu g*g^{-1}$, respectively, which were higher than the apparent C_{max} in other tissues (0.08–0.74 $\mu g*g^{-1}$).

4.2.3. DiI tissue concentration-time profiles after i.v. administration of DME

Different from the rapid plasma clearance after administration of DS and DSE, DiI plasma concentration demonstrated a much slower decrease rate when it was incorporated in the DME (**Figure 4.3**). The estimated initial plasma concentration at time zero was 29.19 $\mu g*mL^{-1}$, which dropped down but then maintained at about 20 $\mu g*mL^{-1}$ during the period of 0.25–1 h, and at about 6–8 $\mu g*mL^{-1}$ during the period of 2–10 h. This prolonged plasma level rendered more chance and/or time of DiI to be distributed and accumulated in various tissues. As the result, high tissue concentrations were observed at late stage, with the concentration-time profile in a few tissues (liver, spleen, small intestine, colon and tumor) not reaching the final elimination phase at the end of the experiment (10 h), the T_{max} in liver, spleen and tumor being 10 h.

DME mainly distributed to the liver, spleen and lungs. The apparent C_{max} in these tissues are in the order of lung > spleen > liver (37.39–20.65 $\mu g*g^{-1}$). These apparent C_{max}s were much higher than the apparent C_{max} in other tissues (0.46–10.01 $\mu g*g^{-1}$), but similar as the estimated C_{max} in plasma (29.19 $\mu g*mL^{-1}$). The apparent C_{max} in heart was 10.01 $\mu g*g^{-1}$, which was in the middle between the apparent C_{max}s of the highly distributed tissues and the slightly distributed tissues ranging from 0.46–3.83 $\mu g*g^{-1}$.

4.2.4. DiI tissue concentration-time profiles after i.v. administration of DLE

From the concentration-time profiles (**Figure 4.4**), it can be seen that after the administration of DLE the plasma concentration decreased from the estimated 0-time 39.43 $\mu g*mL^{-1}$ to about 20 $\mu g*mL^{-1}$ at 0.5 h and then remained around 10–15 $\mu g*mL^{-1}$ during the period of 1–4 h, and thereafter became almost zero. In most tissues, DiI concentration peaked at 2 h, and diminished to almost zero at 6 h, which was correlated with the plasma profile.

The organs with the highest distribution of DiI were spleen, lung and liver. The apparent C_{max} in these organs was 69.44, 41.53 and 28.91 $\mu g*g^{-1}$, respectively, which were higher than the C_{max} in the other tissues (0.66–5.63 $\mu g*g^{-1}$), but close to the estimated apparent C_{max} in plasma (39.43 $\mu g*mL^{-1}$). Among the lowly distributed tissues, the apparent C_{max} in heart and kidney was 5.63 and 4.85 $\mu g*g^{-1}$, respectively, which were still much higher than the apparent C_{max} in brain, colon, small intestine, stomach and tumor (0.66-2.27 $\mu g*g^{-1}$).

In summary, based on the DiI concentration-time profiles in the tissues followed by the intravenous administration of DS, DSE, DME and DLE, a common observation for each formulation was that DiI preferably distributed to the RES organs including the liver, spleen and lungs. The heart and kidneys, on the other hand showed much less DiI accumulation though they are highly perfused. Furthermore, the stomach, small intestine, colon and brain showed limited exposures to DiI, presumably due to the less blood flow or because of the blood brain barrier. Finally, DiI did not show significant distribution in the tumor tissue with the exception of the case by DME administration. In the following sections, further interpretation of the distribution patterns and the comparison among the formulations will be discussed.

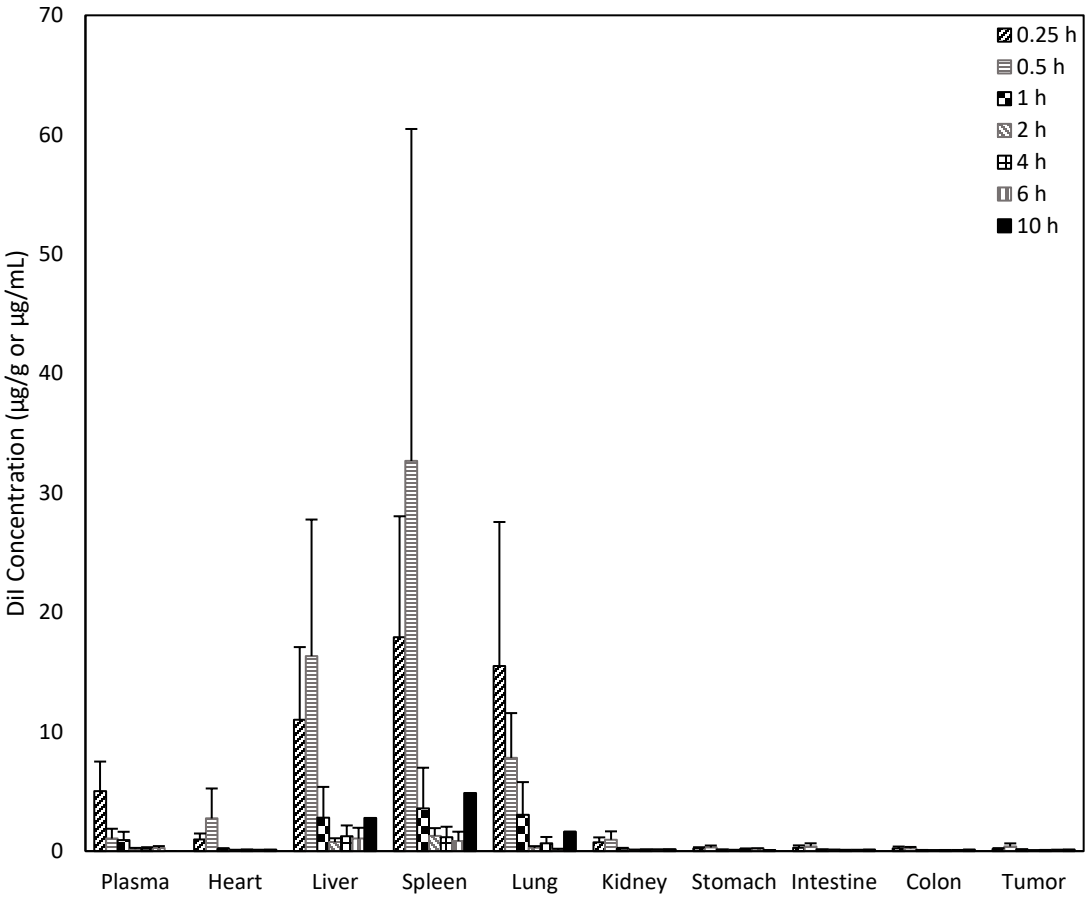

Figure 4.1 DiI tissue concentration-time course after intravenous bolus injection of 5 mg/kg DiI in solution (DS) in C57BL/6J mice (Mean ± SEM, n=3).

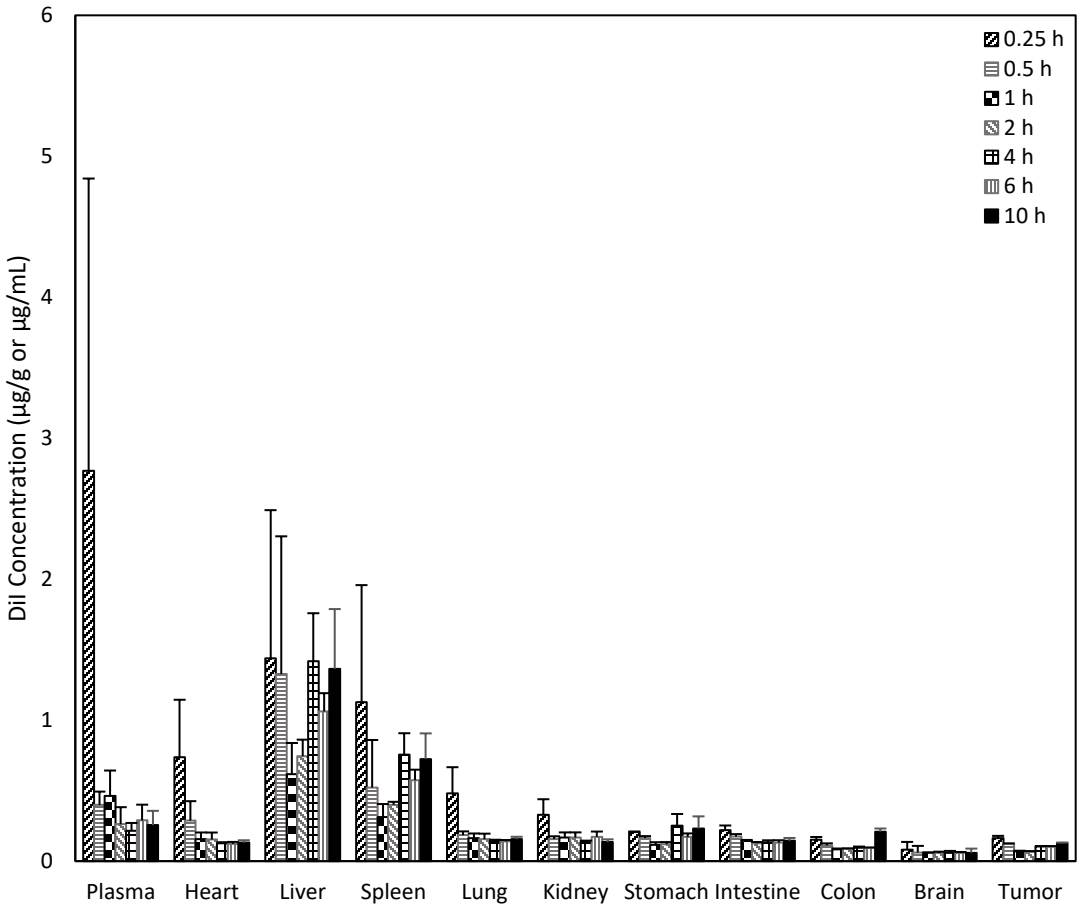

Figure 4.2 DiI tissue concentration time course after intravenous bolus injection of 2 mg/kg DiI loaded in small-size nanoemulsion (DSE) in C57BL/6J mice (Mean ± SEM, n=3).

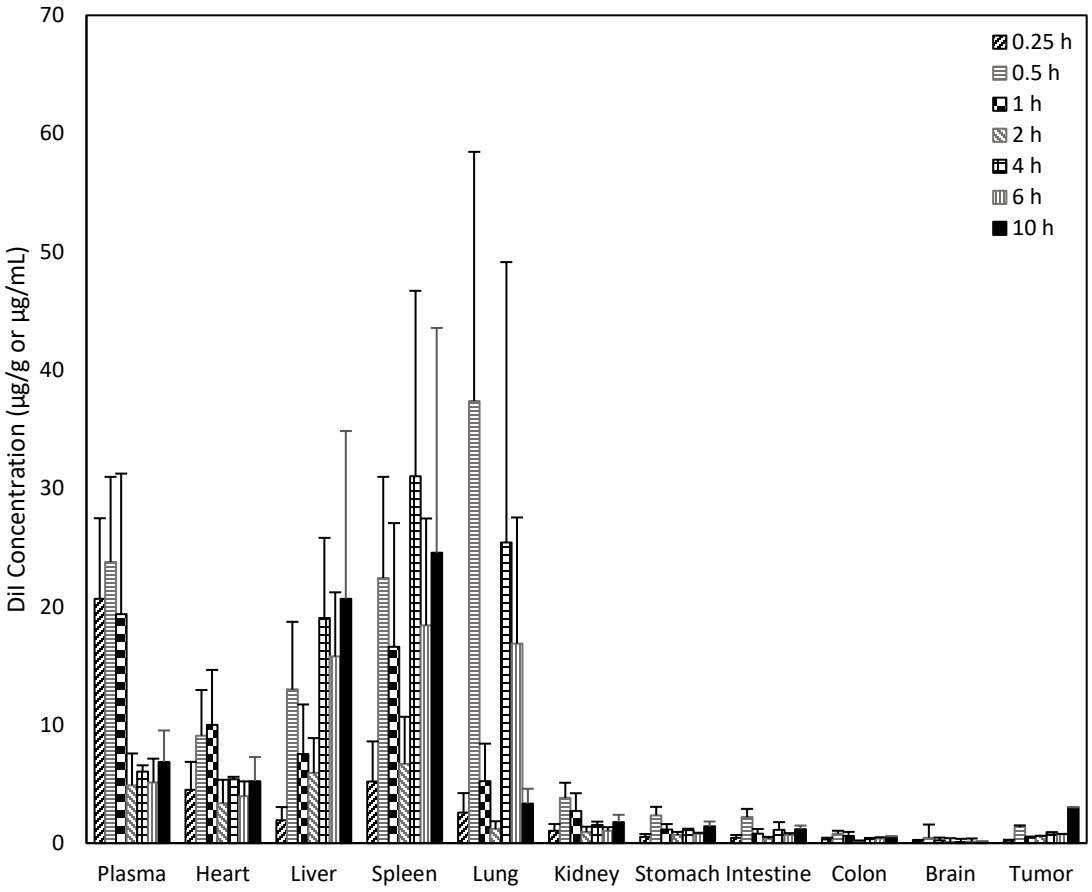

Figure 4.3 DiI tissue concentration time course after intravenous bolus injection of 5 mg/kg DiI loaded in medium-size nanoemulsion (DME) in C57BL/6J mice (Mean ± SEM, n=3).

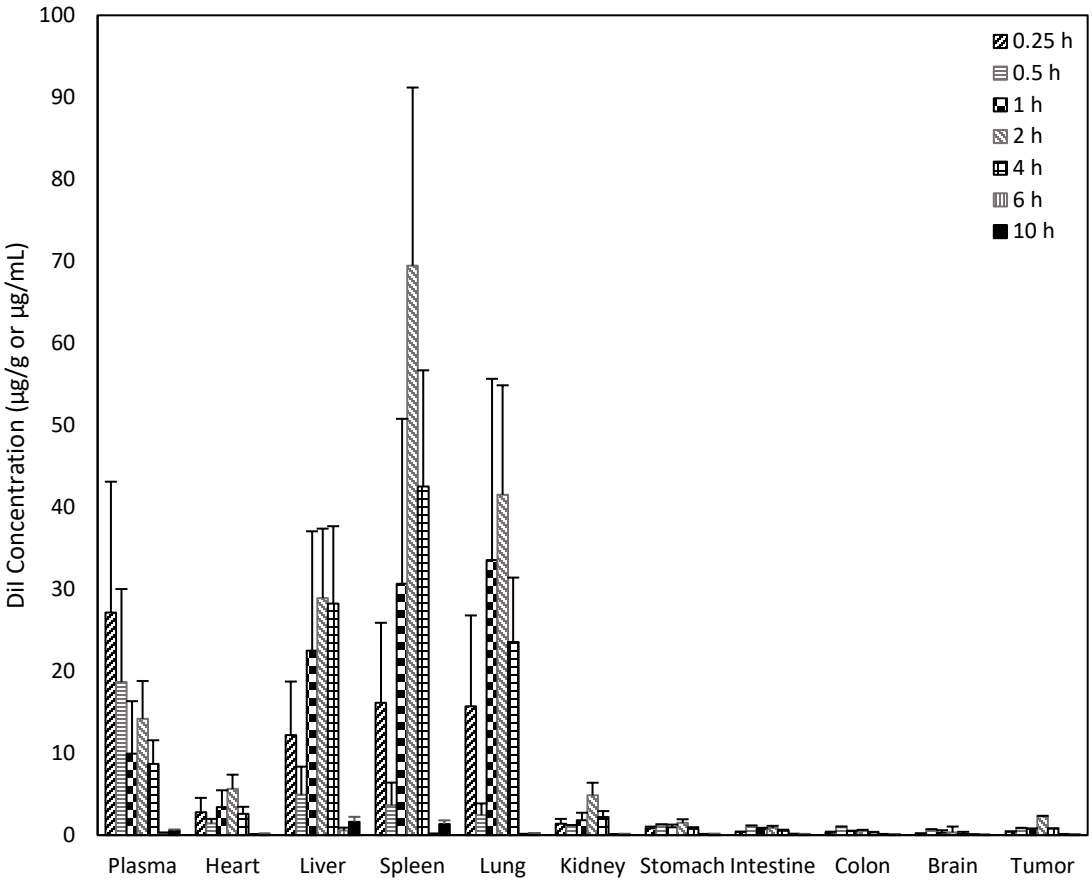

Figure 4.4 DiI tissue concentration time course after intravenous bolus injection of 5 mg/kg DiI loaded in large-size nanoemulsion (DLE) in C57BL/6J mice (Mean ± SEM, n=3).

4.3. The comparison between individual NE versus solution in various tissues

To illustrate the impact of NEs with different droplet sizes and how they alter the PK and biodistribution of the loaded DiI, the DSE, DME and DLE were first individually compared with the free solution. **Figure 4.5** through **Figure 4.15** present the DiI concentration-time profiles of the four formulations in each tissue.

4.3.1. The plasma

Figure 4.5 depicts the plasma profiles after the administration of DS, DSE, DME and DLE. It can be seen that DSE and DS resulted in very similar plasma profiles, with the consideration that the DSE had only less than half of the dose as DS. However, DME resulted in significantly ($p < 0.05$) higher plasma concentrations than DSE and DS at all the sampling time points except for at 1 h (yet about 20-fold higher). And DLE caused the similar plasma profile as DME except at the last two time points, where the plasma concentration decreased almost to zero as the DSE and DS. The phenomenon that the free solution dosage form (DS) resulted in much lower plasma concentration profile than DME and DLE could be due to multiple reasons (the low plasma concentration profile of DSE compared to DME and DLE is discussed in **Sections 4.4.2.**). First and most possibly, the free DiI was rapidly cleared from the plasma. As discussed previously, the liver, spleen and lungs already showed higher DiI concentrations at 0.25 h than that of the plasma indicating a fast distribution had occurred. The extrapolated C_{max} at time 0 for DS, DME and DLE was 24.01, 29.19 and 39.43 µg/mL, respectively. These similar 0–time concentrations were expected as the doses were same. However, there were significant differences in concentrations at 0.25 h and further time points indicate the possibility of the fast plasma clearance of DiI given as free solution. Secondly, a portion of DiI in the ethanol solution could immediately precipitated

because of the quick dilution in the blood after administration. Another possibility was that a portion of DiI partitioned into the cellular components of the blood which was therefore excluded from the plasma assay. But this was unlikely to happen when DS was given due to the slow staining rate of the dye into live tissues, not to mention in the dynamic flow of the blood stream (Invitrogen, 2010).

4.3.2. The heart

As shown in **Figure 4.6**, DiI peaked fast within 0.5 h followed by a rapid clearance from the heart resulting negligible concentration after 1 h when given in the DS. DSE demonstrated comparable concentration course in the heart as DS. Contrarily, DME and DLE, especially the former one, increased significantly the apparent C_{max} of DiI in the heart, being 1.1-fold and 2.7-fold increase for DLE and DME, respectively. Since the heart is mostly comprised of myocardium and the blood perfusion is the major determinant for drug distribution into its tissue, the drug concentration in the heart usually correlates well with the corresponding heart concentration when given as the free solution form. The modification by drug delivery system could sometimes lead to the change in the PK of the drug in the heart, such as the case of the liposomal Doxorubicin (Papahadjopoulos et al., 1991). In the current study, increased DiI concentration was observed in the heart at each time point followed by DME administration, compared to the solution or other NEs. To the best of our knowledge, there lacks literature report on the heart distribution of NEs prepared with HS. It has been reported, however, that HS based micellar solutions altered the encapsulated drugs heart disposition as compared to the free drug solutions, though the results were somewhat contradictory (Ma et al., 2012; Lu et al., 2014). Therefore, at this point, it is hard to give an explanation on the favorable heart accumulation by DME. Nevertheless, this

observation is worth of further investigation and could possibly arise as a heart targeting drug delivery strategy.

4.3.3. The liver, the spleen and the lungs

The comparison for distribution in the liver, spleen and lungs tissues are grouped and discussed together (**Figure 4.7**, **4.8** and **4.9**), as they are all highly perfused and also abundant with the RES thereby responsible for the particulate matters clearance, though the lungs play this role to a lesser extent (Baas et al., 1994). Indeed, DiI was mainly recovered from these tissues regardless of the formulations. However, when DME and DLE were administered, there was a further remarkable increase of the DiI distribution in these tissues as compared to the DS.

It is interesting to see that the pattern of the concentration-time profile following DS administration was different from those after DME and DLE administration. The apparent peak concentration after DS administration occurred at 0.25 h (lung) and at 0.5 h (liver and spleen), and then rapidly decreased to negligible level at 2 h. This was probably due to 1) fast distribution of DiI as in a solution form into these tissues, and 2) DiI precipitated out after dosing in the blood circulation and the precipitate was captured by the RES system. And then DiI was quickly metabolized in these organs, especially maybe in the liver. The apparent peak concentration after DME and DLE administration reached at later time period than DS, which represented gradual accumulation in the organs of DiI when delivered in NE form which prolonged the residence time in the blood circulation. This was supported by the comparison of apparent plasma C_{max}s, since compared to DS, DME and DLE increased the plasma C_{max} only 1.2- and 1.6-folds, respectively (**Figure 4.16**).

Another interesting finding was observed from DSE. As mentioned earlier, unlike DME and DLE, DSE did not achieve significant increase in plasma exposure as compared to DS. In fact,

DSE actually decreased spleen and lungs exposures as compared to DS. The apparent C_{max} in the liver, spleen and lungs decreased by 78%, 91.4% and 92.3%, respectively. In addition, DiI was not significantly recovered from the other tissues after DSE administration. The following discussion may help to explain this phenomenon.

As demonstrated by Braet et al., noncontinuous endothelia with vascular fenestrations measuring 50 to 100 nm is present in the liver which leads to nonspecific accumulation of particles larger than that (Braet et al., 2007). Similarly, splenic filtration accounts for retention of particles bigger than 200 nm, due to the 200-500 nm size range of inter-endothelial cell slits (Chen and Weiss, 1973). The lung capillaries have even larger size cutoff in the micrometer range (2 to 5 μm). Although these are human anatomy parameters and no mouse parameters are found in the literature, it could be reasoned that the ~30 nm DSE might pass through the intercellular fenestrations in these mouse tissues freely, resulting significant lower accumulation. The present finding is in agreement with Attia et al. in whose study the NE with 55-nm size yielded reduced *in vivo* hepatic toxicity in rats and the authors attributed this to the reduced cellular uptake of the NE observed *in vitro* (Attia et al., 2016).

4.3.4. The kidneys

The distribution of DiI into the kidneys was generally low for all the formulations. DLE achieved the highest apparent C_{max} around 5 $\mu g*g^{-1}$, followed by DME (~4 $\mu g*g^{-1}$), DS (~1 $\mu g*g^{-1}$) and DSE (<1 $\mu g*g^{-1}$). The apparent T_{max} was 0.25, 0.5, 0.5 and 2 h for DSE, DS, DME and DLE, respectively. DME maintained the concentration within the range of 0.94-1.77 $\mu g*g^{-1}$ during the period of 6-10 h, while the other three resulted in negligible concentrations.

4.3.5. The stomach, the small intestine, the colon and the brain

The rest body tissues under investigation including the gastrointestinal tract (GIT) tissues and the brain were grouped and discussed together as they all showed limited DiI exposure (**Figure 4.11** through **Figure 4.14**). DS resulted in the concentration in the range of 0.11-0.40 $\mu g*mL^{-1}$ in all the GIT tissues. DSE resulted in the concentration range in the GIT tissues similar to that by DS. DME and DLE achieved relatively higher concentration than DS, but still only in the range of 0.30-2.35 $\mu g*g^{-1}$ in the GIT tissues. Compared to DS, DME increased the apparent C_{max} in the GIT tissues by 2.5-6.8 folds, and DLE achieved 1.8-4.0- fold increase. The overall low DiI distribution into these GIT tissues was probably because of the low blood perfusion.

The distribution of DiI in the brain tissue was even lower than that in the GIT tissues for all the three NEs, with the majority concentrations being less than 0.2 $\mu g*g^{-1}$. The apparent C_{max} by DME and DLE was 0.46 and 0.66 $\mu g*g^{-1}$, respectively, while only 0.1 $\mu g*g^{-1}$ by DSE. Since the brain DiI concentration after the administration of the DS was not determined, it is impossible to compare DS vs the three NEs. Nevertheless considering the brain has a moderate to high blood perfusion similar as that of the liver (Gjedde and Gjedde, 1980), the absolute low DiI distribution in brain after the i.v. administration of the NEs indicates that the blood brain barrier (BBB) played a major role to prevent the NE droplets from entering the central nervous system (CNS).

4.3.6. The tumor

In the current study, DiI accumulation in the subcutaneous B16F10 melanoma was also studied to evaluate the potential formulation benefit for the enhanced tumor targeting effect. In general, the distribution of DiI in the tumor was low for all the formulations. DSE resulted in similar concentration profile (below 0.5 $\mu g*g^{-1}$ throughout the entire experimental time) as DS. DLE

caused a 4.8--fold increase in apparent C_{max}, as compared to DS. DME further profoundly enhanced DiI tumor disposition demonstrated by a 7.7- fold improved $C_{max.}$ Notably, DiI peaked in the tumor at 2 h post the injection of DLE and then dropped to negligible level at 6 h and 10 h. However, following DME administration, the accumulation in tumor continued to the last sampling point, resulted in the highest concentration (3.01 $\mu g*g^{-1}$) at the end of the experiment.

It has been well known that to fully utilize the EPR effect for NPs accumulation in tumor through passive diffusion, the prerequisites are first an optimal particle size to exert enhanced permeation as well as reduced lymphatic drainage, and secondly a sufficiently long circulation time to carry out such accumulation (Ma et al., 2012). As DME possesses both of the features of ~200 nm in size and the longest plasma circulation evidenced by the significant higher plasma concentration at the last sampling point, it indeed showed the most significant tumor uptake as compared to the other three dosage forms.

As the summary of **Section 4.3**, NEs altered the biodistribution of DiI to various degrees. Compared to DS, DSE caused a minimum increase in biodistribution in some tissues but decrease in other tissues. However, DME and DLE enhanced the biodistribution in all tissues with remarkable increase in several tissues. Therefore, in the next section, the three NEs are compared to further elucidate the formulation impact on the NE biodistribution patterns.

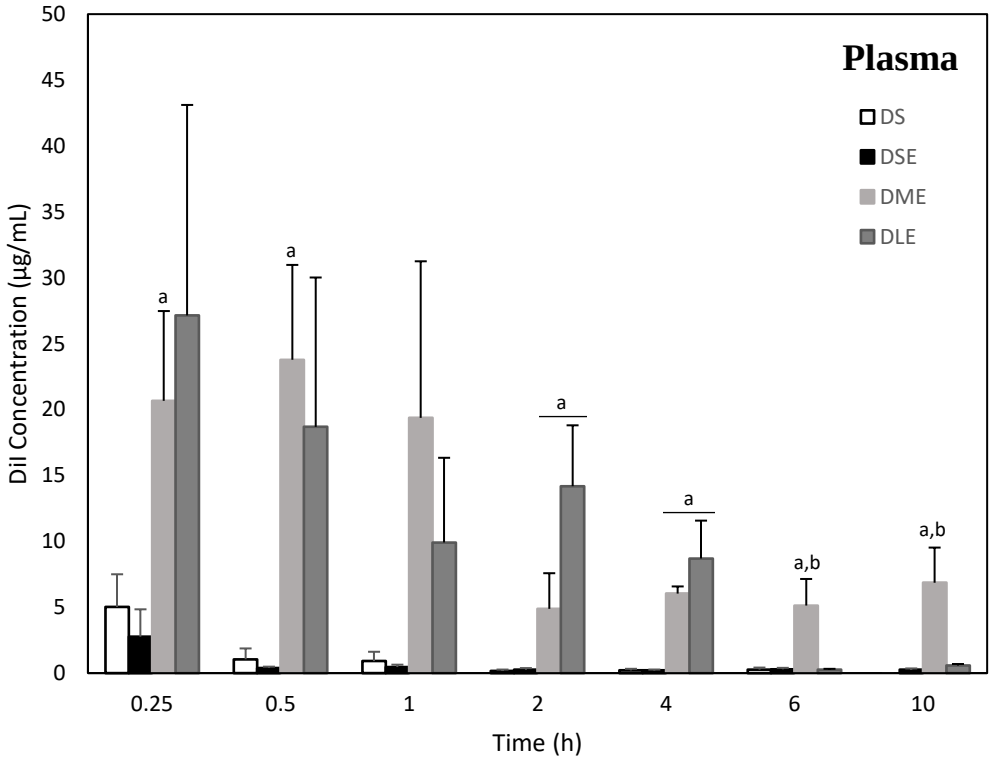

Figure 4.5 DiI concentration-time course in the plasma after intravenous bolus injection of DiI solution (DS, 5 mg DiI/kg), small-size nanoemulsion (DSE, 2 mg DiI/kg), medium-size nanoemulsion (DME, 5 mg DiI/kg) and large-size nanoemulsion (DLE, 5 mg DiI/kg). (Mean ± SEM, n=3; Significantly different from DS (a) and DLE (b), $p < 0.05$)

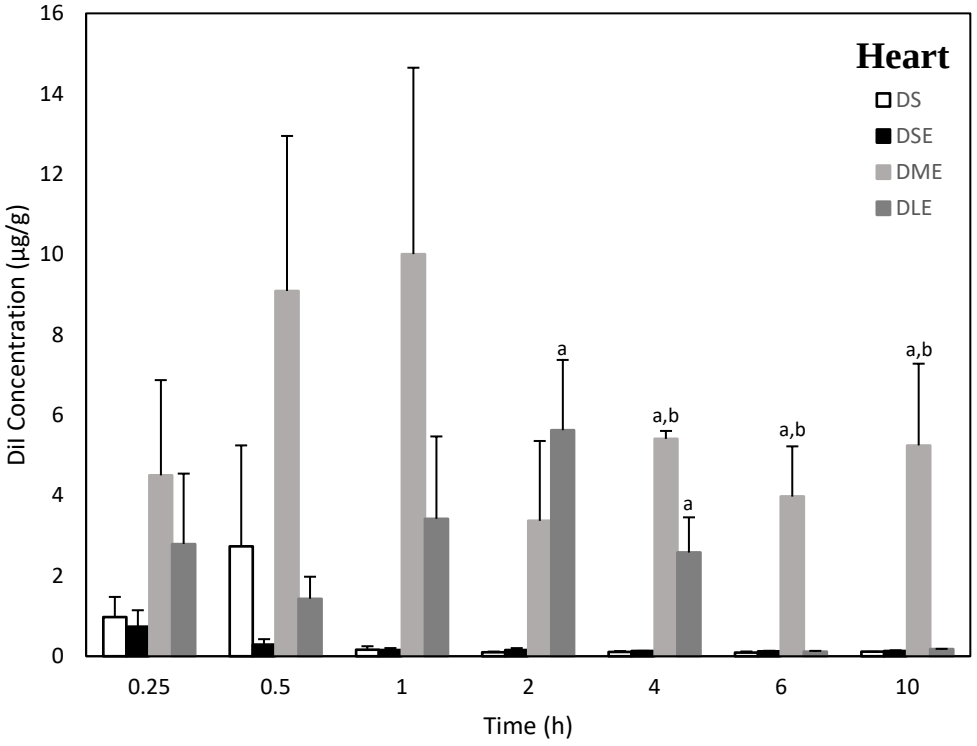

Figure 4.6 DiI concentration-time course in the heart after intravenous bolus injection of DiI solution (DS, 5 mg DiI/kg), small-size nanoemulsion (DSE, 2 mg DiI/kg), medium-size nanoemulsion (DME, 5 mg DiI/kg) and large-size nanoemulsion (DLE, 5 mg DiI/kg). (Mean ± SEM, n=3; Significantly different from DS (a) and DLE (b), $p < 0.05$)

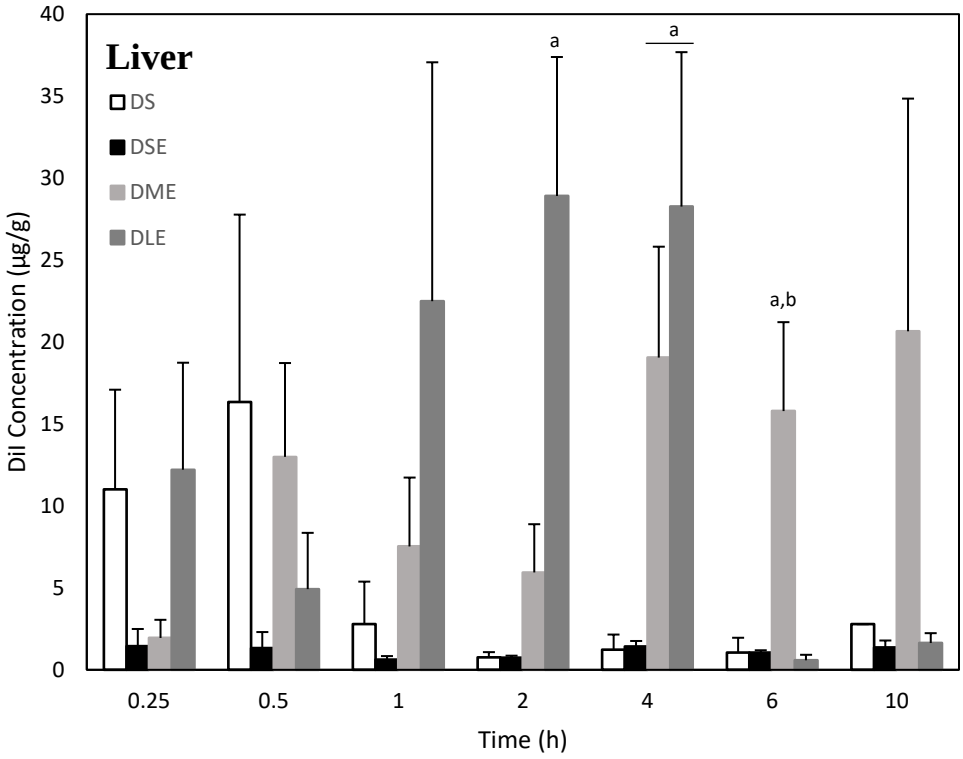

Figure 4.7 DiI concentration-time course in the liver after intravenous bolus injection of DiI solution (DS, 5 mg DiI/kg), small-size nanoemulsion (DSE, 2 mg DiI/kg), medium-size nanoemulsion (DME, 5 mg DiI/kg) and large-size nanoemulsion (DLE, 5 mg DiI/kg). (Mean ± SEM, n=3; Significantly different from DS (a) and DLE (b), $p < 0.05$)

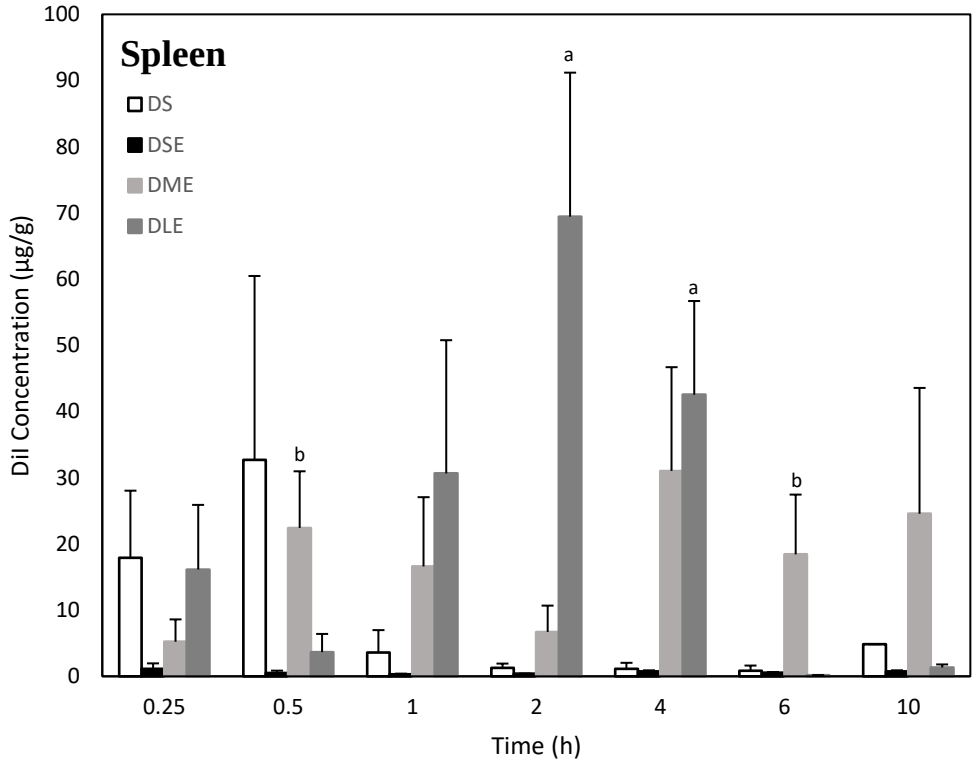

Figure 4.8 DiI concentration-time course in the spleen after intravenous bolus injection of DiI solution (DS, 5 mg DiI/kg), small-size nanoemulsion (DSE, 2 mg DiI/kg), medium-size nanoemulsion (DME, 5 mg DiI/kg) and large-size nanoemulsion (DLE, 5 mg DiI/kg). (Mean ± SEM, n=3; Significantly different from DS (a) and DLE (b), $p < 0.05$)

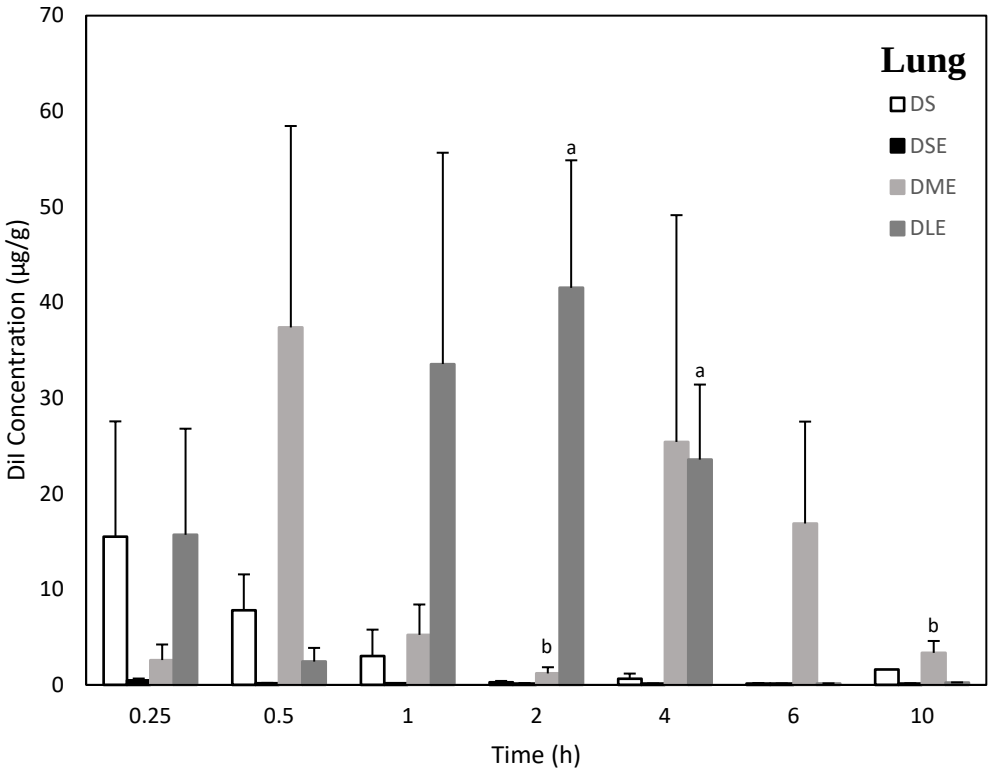

Figure 4.9 DiI concentration-time course in the lungs after intravenous bolus injection of DiI solution (DS, 5 mg DiI/kg), small-size nanoemulsion (DSE, 2 mg DiI/kg), medium-size nanoemulsion (DME, 5 mg DiI/kg) and large-size nanoemulsion (DLE, 5 mg DiI/kg). (Mean ± SEM, n=3; Significantly different from DS (a) and DLE (b), $p < 0.05$)

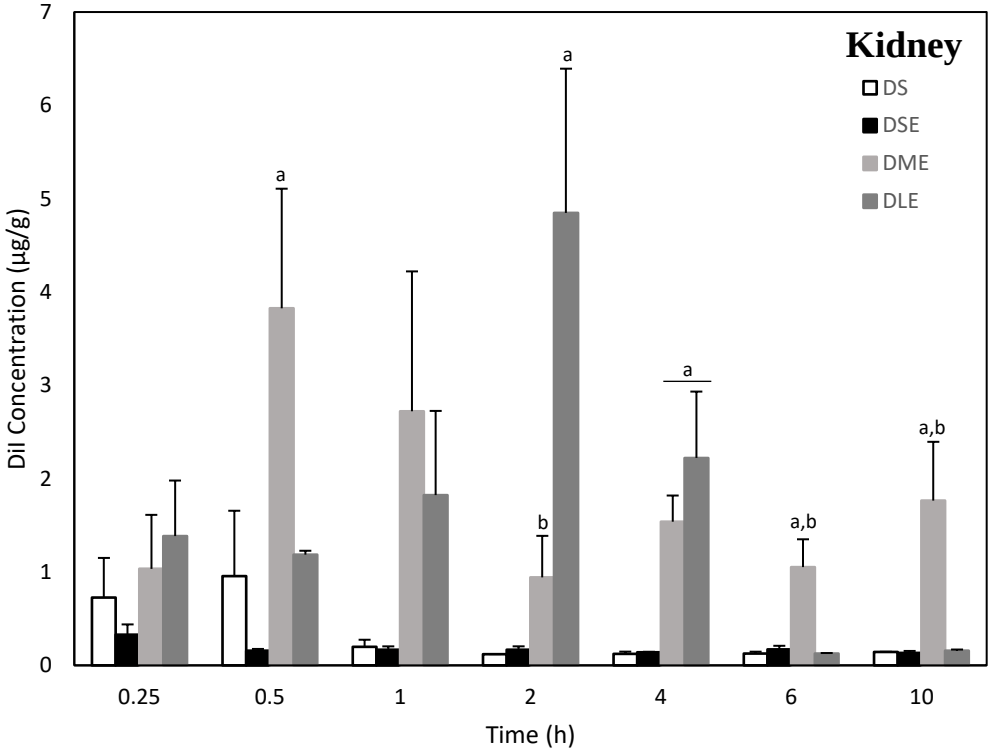

Figure 4.10 DiI concentration-time course in the kidneys after intravenous bolus injection of DiI solution (DS, 5 mg DiI/kg), small-size nanoemulsion (DSE, 2 mg DiI/kg), medium-size nanoemulsion (DME, 5 mg DiI/kg) and large-size nanoemulsion (DLE, 5 mg DiI/kg). (Mean ± SEM, n=3; Significantly different from DS (a) and DLE (b), $p < 0.05$)

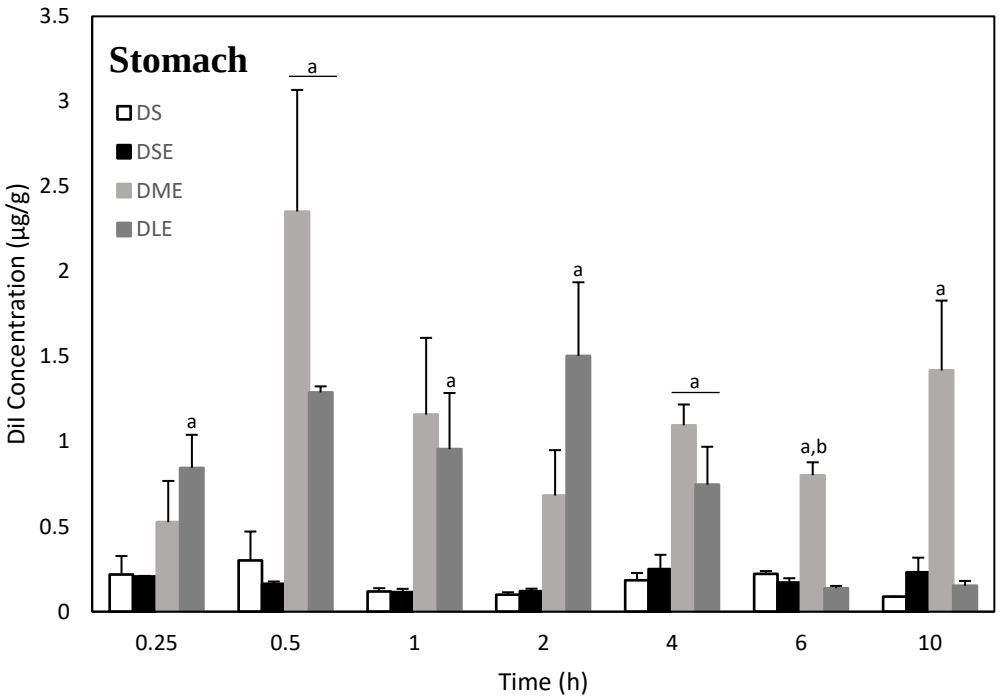

Figure 4.11 DiI concentration-time course in the stomach after intravenous bolus injection of DiI solution (DS, 5 mg DiI/kg), small-size nanoemulsion (DSE, 2 mg DiI/kg), medium-size nanoemulsion (DME, 5 mg DiI/kg) and large-size nanoemulsion (DLE, 5 mg DiI/kg). (Mean ± SEM, n=3; Significantly different from DS (a) and DLE (b), $p < 0.05$)

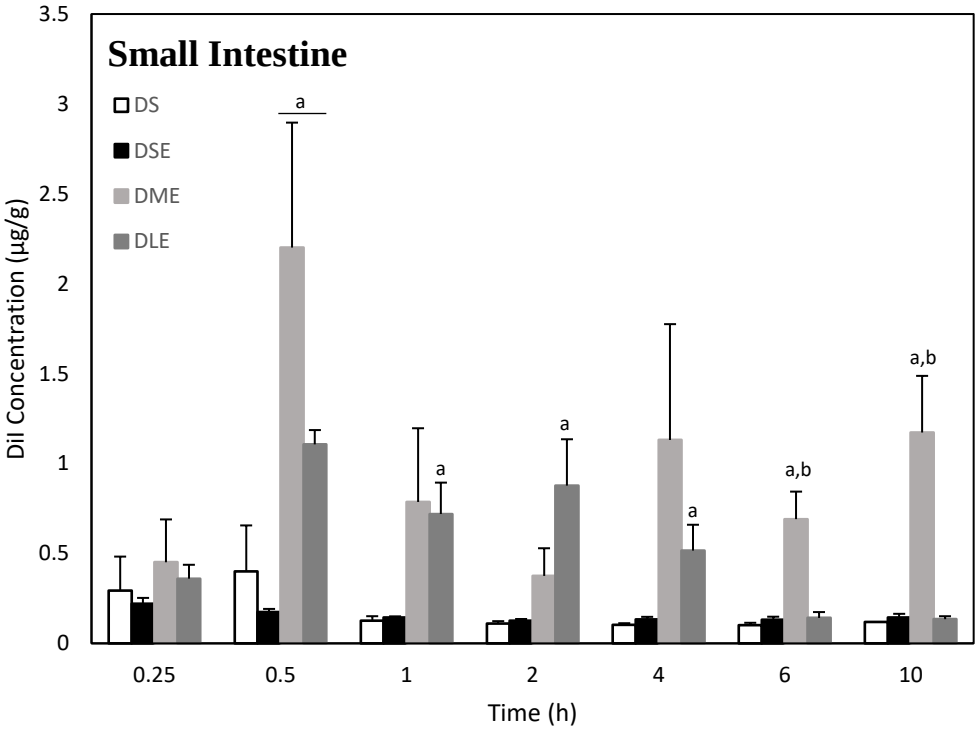

Figure 4.12 DiI concentration-time course in the small intestine after intravenous bolus injection of DiI solution (DS, 5 mg DiI/kg), small-size nanoemulsion (DSE, 2 mg DiI/kg), medium-size nanoemulsion (DME, 5 mg DiI/kg) and large-size nanoemulsion (DLE, 5 mg DiI/kg). (Mean ± SEM, n=3; Significantly different from DS (a) and DLE (b), $p < 0.05$)

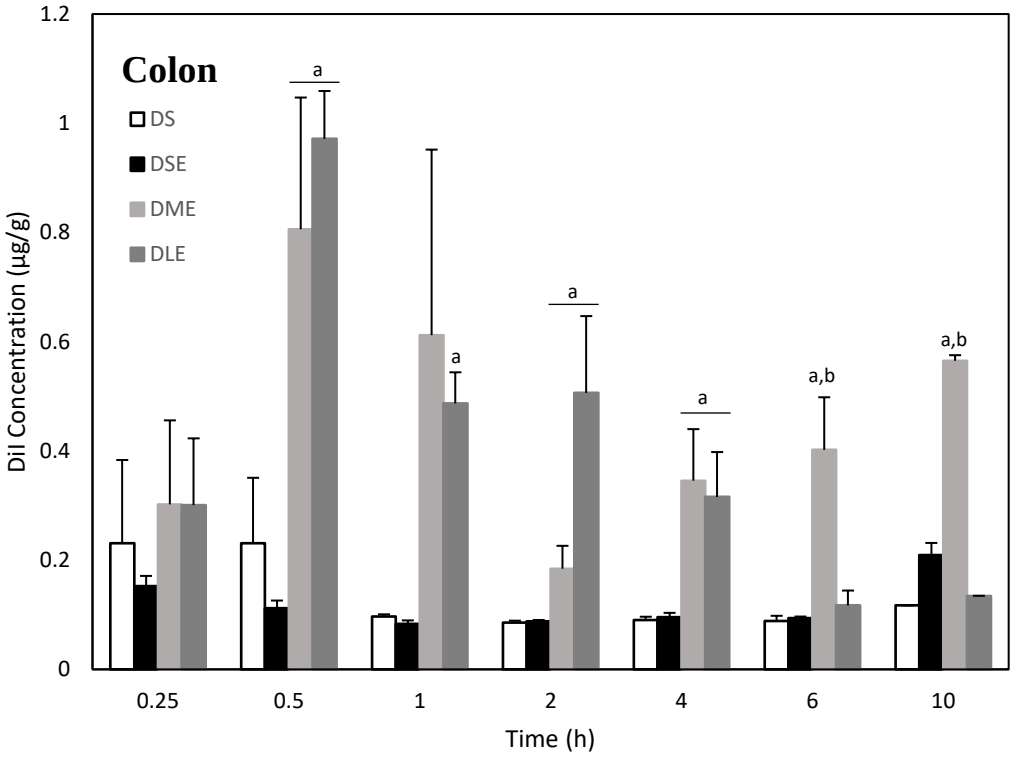

Figure 4.13 DiI concentration-time course in the colon after intravenous bolus injection of DiI solution (DS, 5 mg DiI/kg), small-size nanoemulsion (DSE, 2 mg DiI/kg), medium-size nanoemulsion (DME, 5 mg DiI/kg) and large-size nanoemulsion (DLE, 5 mg DiI/kg). (Mean ± SEM, n=3; Significantly different from DS (a) and DLE (b), $p < 0.05$)

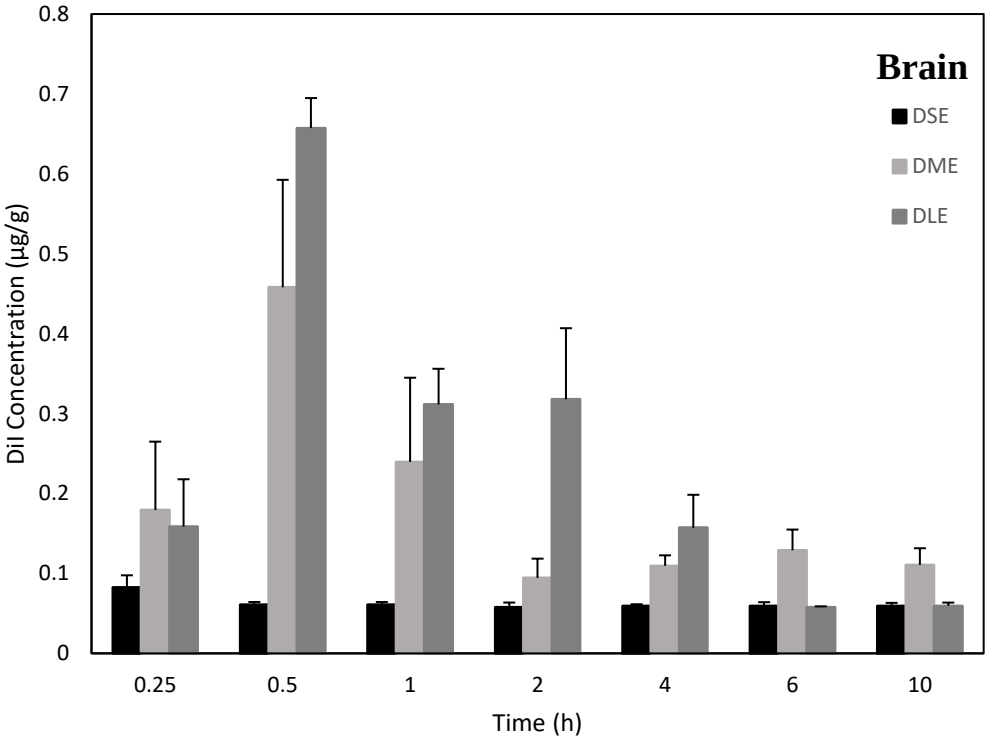

Figure 4.14 DiI concentration-time course in the brain after intravenous bolus injection of small-size nanoemulsion (DSE, 2 mg DiI/kg), medium-size nanoemulsion (DME, 5 mg DiI/kg) and large-size nanoemulsion (DLE, 5 mg DiI/kg). (Mean ± SEM, n=3)

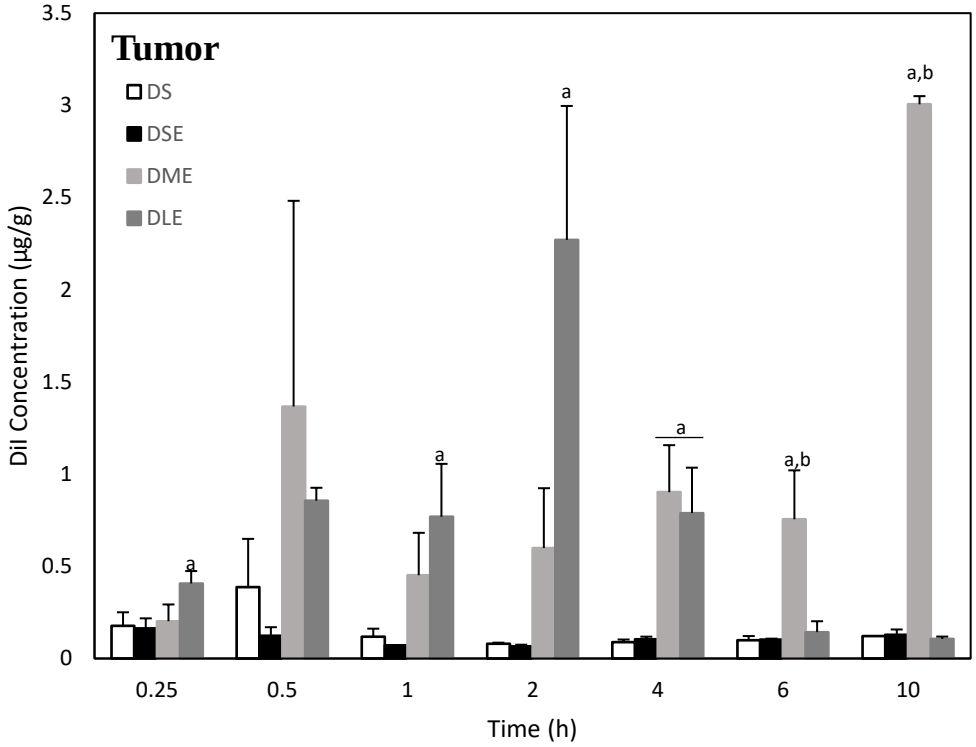

Figure 4.15 DiI concentration-time course in the tumor after intravenous bolus injection of DiI solution (DS, 5 mg DiI/kg), small-size nanoemulsion (DSE, 2 mg DiI/kg), medium-size nanoemulsion (DME, 5 mg DiI/kg) and large-size nanoemulsion (DLE, 5 mg DiI/kg). (Mean ± SEM, n=3; Significantly different from DS (a) and DLE (b), $p < 0.05$)

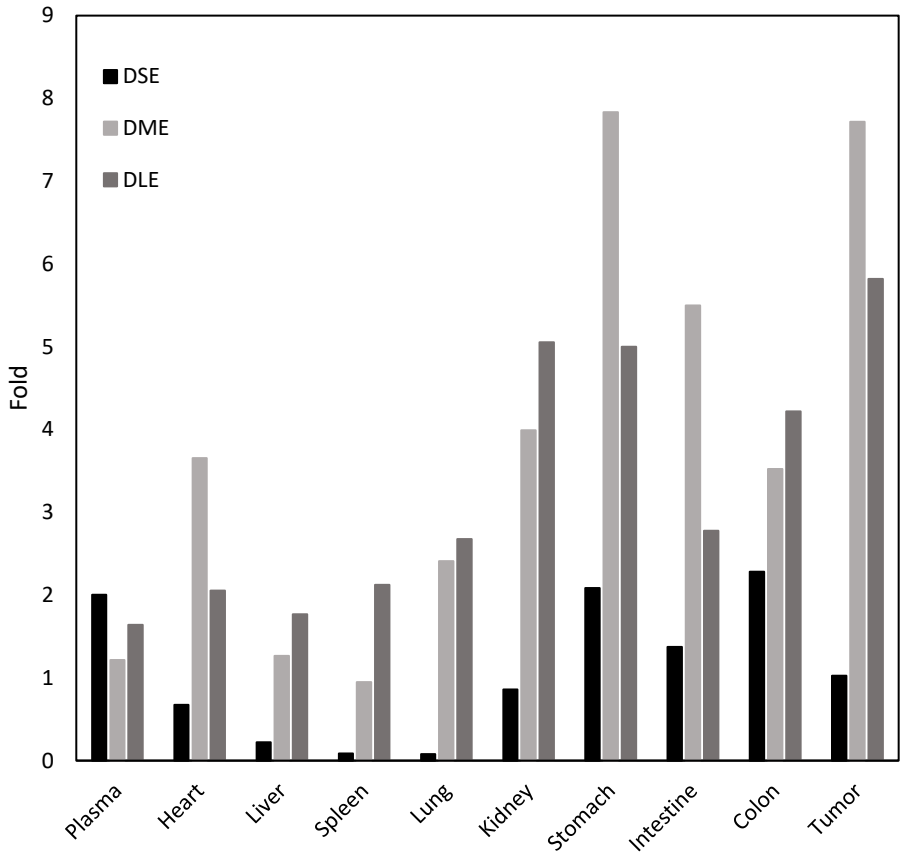

Figure 4.16 The comparison of dose normalized DiI apparent maximum concentrations (C_{max}) in various tissues after intravenous bolus injection of DiI loaded small-, medium- and large-size nanoemulsion (DSE, DME and DLE) versus DiI solution (DS), respectively.

4.4. Discussions on O/W NE biodistribution upon intravenous administration

4.4.1. Potential factors contributed to the NE biodistribution

In the literature, extensive research has been conducted to study the factors which may impact the PK and biodistribution of solid NPs. The particle size, shape/morphology, surface charge, PEGylation and targeting ligands of the NP are widely known factors which determine the *in vivo* behavior of the NPs (Alexis et al., 2008; Ernsting et al., 2013; Blanco et al., 2015). Therefore, it is necessary to discuss the variables involved in the current study which might contributed to the NEs biodistributions.

Firstly, the shape of the liquid droplets was spherical in nature which should not be a concern. Secondly, the non-ionic surfactant HS was used without other ligands associated throughout all the NEs in the current study. The exclusive use of HS herein as the sole surfactant helped to minimize the effect from the droplet surface related variables. Notably, unlike solid NPs, it was not practical to obtain NEs with different droplet sizes yet at same surfactant concentrations, hence the inconsistent PEG concentration on the droplet surface of the developed NEs could have impact on their biodistributions.

Besides the previous factors, the number of the droplets administered could also be a variable thus deserves a discussion. It has been reported that the highest ever tested single injected lipid dose for Intralipid® 10% was 10 g/kg (i.e., 1% mice weight) which was well tolerated by the mice, and because of that even higher dose was irrelevant to be tested (Product monograph for INTRALIPID® lipid injectable emulsion). This could probably explain why the approaches taken in the literature when studying the NPs size effect on biodistribution universally used constant drug/dye dose or surface area rather than the number of the NPs, as the number of NPs commonly administered falls far below the threshold the animals could tolerate. Similarly, the total lipid

used in the current study did not exceed 0.2% of the mice body weight, which makes it reasonable to assume that the lipid given also follows linear kinetics where the number of droplets would not impact on distribution. Moreover, the comparison of the three NEs in the current study shows no correlation between biodistribution and number of droplets. In general, the trend of the biodistribution change from DSE (with largest number of droplets) to DME was opposite to that from DME to DLE (with fewest number of droplet). For example, both DSE and DLE exhibited lower heart concentrations than DME.

Based on the above discussion, the biological fate of the studied NEs should therefore be possibly impacted by their droplet size and the surface PEG density combinedly and the factors are related to each other and cannot be completely separated.

4.4.2. The biodistribution of SE

As discussed previously, though DSE had a dose normalized apparent C_{max} comparable to other NEs, it contrarily showed limited plasma exposure. Neither did it accumulate in the RES tissues including the liver, spleen and lungs. In addition, the other tissues under investigation did not manifest major DiI recovery. Hence, the question where DSE has distributed in the body needs an answer. Since the renal filtration cutoff size is 5.5 nm (Choi et al., 2007) and even considering the mice kidney glomeruli pore radius as large as 9.6 nm (Jeansson and Haraldsson, 2003), DSE is still much larger in size which excludes the possibility by glomerular filtration. Herein, the following two kinds of possible *in vivo* fate of DSE are proposed.

Moghimi et al. demonstrated that the endothelium of bone marrow sinusoids could remove particles from circulation by intercellular routes through the fenestrate in the endothelial wall and this route was strongly dependent on the particle size (Moghimi, 1995) because the size of the

fenestrate was reportedly 85-150 nm (Huang, 1971). Non-targeting liposomes were demonstrated to accumulate three-fold higher in bone marrow of dog when their size was reduced from 1200 to 400 nm (Schettini et al., 2006). Similarly, non-ionic poloxamer-407 coated polymeric NPs less than 150 nm in size were found to have an enhanced bone marrow disposition in rabbits (Porter et al., 1992). As DSE is much smaller than these NPs in the literature, chances were that the majority of the droplets could pass through the fenestrations presented in the RES organs which resulted in the reduced accumulation in these tissues. Also considering the blood flow rate through the capillary bed in the bone marrow is 51 $mL*(100\ g)^{-1}*min^{-1}$ in the rabbit (Cumming, 1962) which is as rapid as the perfusion of 54 $mL*(100\ g)^{-1}*min^{-1}$ into the brain (Kety and Schmidt, 1946), DSE could possibly show significant disposition in the bone marrow.

The second hypothesis is associated with the fenestrations presented in the blood vessel epithelium. There are three main types of endothelium: continuous (lacking fenestrations), fenestrated and discontinuous (Risau, 1998; Robert and Palade, 2000). The fenestrations are more abundant in the endothelium of organs where a higher rate of exchange between intra- and extravascular compartments is required, such as in the gastrointestinal or peritubular renal capillaries (Simon and Filip, 2009). These fenestrations retain permeability to the macromolecules to some extent, and especially in discontinuous endothelia, larger fenestrations may allow passage of lipid particles such as chylomicrons (75-600 nm) and cellular debris (Levick and Smaje, 1987). Once these entities pass through the fenestra, they would be collected by the nearby lymphatic vessels to the lymph nodes or circulating in the lymphatic system. Thereby, DSE droplets could undergo this pathway and end up in the lymphatic system. Yet these speculations require further investigation.

4.4.3. The biodistribution of ME and LE

DME and DLE both resulted in substantially distinct concentration-time profiles in the various tissues from DSE, but similar to each other with some differences. To further illustrate how DME and DLE altered the biodistribution of DiI, the point-to-point comparison of the tissue concentration ratio at each sampling time were utilized and the results are presented in **Table 4.1**. The advantage of this approach was that it did not rely on any assumption, yet practically the concentration in specific tissues is the determinant factor for the pharmacodynamic (PD) effect for most of the drugs. Furthermore, statistical analysis could also be performed.

As shown in **Table 4.1**, the mean concentrations in the tissues by DME and DLE were first compared statistically. Values presented with underscore indicate the significant differences at 95% confidence. Due to the large variations, many comparisons did not yield statistical differences though the mean value suggested potential difference. The increase of sample size could possibly address the issue. Herein though, the biodistribution pattern was analyzed by the color coding. The mean tissue concentration ratios of DME:DLE were grouped by four regions. A more than 2-fold in favor of DME was red-shaded, followed by the yellow area of favored DME but within 2-fold, then the blue area of favored DLE within 2-fold and lastly the blank area of favored DLE with more than 2-fold. The results demonstrated foremost that DME distributed in various tissues universally higher than DLE at 0.5 h and from 6 h and on. This non-specific enhanced tissue exposure should be due to the earlier peak at 0.5-1 h and the prolonged blood circulation of DME. On one side, it could be a useful formulation to deliver lipophilic anticancer drugs to the tumor by EPR; opposingly, as elaborated by Bittner, the change in PK by HS especially its non-specific high organ dispositions could possibly increase the encapsulated drugs toxicity (Bittner et al., 2003). This side effect could be elevated in certain tissues such as the heart based on our observation. As suggested by the color coding, DME had a higher heart distribution

compared to DLE almost throughout the test period. Secondly, DLE peaked at 2 h which caused a higher concentration in all the tissues than DME though this peak rapidly decreased ever since. Thirdly, the clear region of the liver, spleen and lungs from 0.25 to 2 h (except for 0.5 h) indicates a favorable distribution into these tissues by DLE and such pattern could be extended to 4 h just with less extent. As discussed previously, the vascular fenestration of the endothelia presented in the liver and spleen serves as a passive "mesh" (Braet et al., 2007; Chen and Weiss, 1973). Therefore, the larger droplet of DLE could be much easily trapped in these tissues whilst DME alleviated such effect due to the closeness of size to the cutoff. The reticuloendothelial system (RES) is also responsible for clearing particulate matters such as bacteria, fungi, viruses and dying cells from the circulation (Aschoff, 1924). As the droplet size increases, chances are that they could be more easily recognized thus subsequently end up mainly in the liver, spleen and lungs which are the major constituents of RES.

Table 4.1 The tissue mean concentration ratio of DME versus DLE

Tissue	Time (h)						
	0.25	**0.5**	**1**	**2**	**4**	**6**	**10**
Plasma	0.761	1.273	1.953	0.344	0.694	*19.884	11.926
Heart	1.611	6.352	2.927	0.599	2.096	34.259	29.989
Liver	0.159	2.639	0.335	0.206	0.674	27.214	12.647
Spleen	0.324	6.127	0.542	0.097	0.729	115.887	18.333
Lung	0.166	15.331	0.156	0.029	1.078	109.623	13.094
Kidney	0.747	3.226	1.493	0.195	0.693	8.357	11.177
Stomach	0.622	1.825	1.213	0.454	1.467	5.854	9.268
Intestine	12.528	1.990	1.095	0.427	2.192	4.901	8.681
Colon	1.000	0.830	1.257	0.364	1.095	3.436	4.216
Brain	1.126	0.697	0.772	0.296	0.701	2.224	1.881
Tumor	0.496	1.597	0.588	0.264	1.143	5.280	28.358

* Value presented with underscore indicates a significant difference at $P < 0.05$ (n=3).

DME/DLE: >2 (red), 1-2 (yellow), 0.5-1 (blue) and <0.5 (blank).

4.5. Summary

DiI concentration-time profiles in various tissues were obtained after intravenous injection of DS, DSE, DME and DLE. The characteristics of the biodistribution pattern of the studied NEs are summarized in **Table 4.2**.

Table 4.2 The characteristics of the studied NE biodistributions

	Small-size NE (~30 nm)	**Medium-size NE (~200 nm)**	**Large-size NE (~900 nm)**
Plasma circulation	Not prolonged	Significantly prolonged	Not prolonged
Plasma concentration	Low	High	Intermediate
RES organs (Liver, spleen and lungs) accumulation	Very low	Significantly enhanced, more profound in a long period of time	Highly enhanced in the early hours, rapidly cleared then
Preferably distributed organ	Not found	The RES organs and the heart	The RES organs especially the spleen and the lungs
Subcutaneous tumor accumulation	Not significant	Highly enhanced	Intermediately enhanced

Chapter 5. Conclusion and perspectives

In this chapter:

- The current study is concluded and
- Some perspectives originated from this study are provided.

5.1. Conclusion

In the current study, DiI loaded NEs with defined droplet sizes (~30, 200 and 900 nm) were prepared and tested *in vivo* for their biodistributions in C57BL/6J mice. The biodistributions of the NEs were impacted by their droplet size and surface PEG density. DSE did not show significant exposure to the tissues of interest and the biological fate required further investigations. DME showed a prolonged blood circulation, non-specific higher tissue accumulation than the other size NEs especially in the heart and tumor. DLE demonstrated a preferable accumulation in the liver, spleen and lung and subsequently quickly cleared from these organs.

5.2. Perspectives

Our current study has explored the intravenous NEs *in vivo* biodistribution patterns in C57BL/6J mice. The results suggest that the droplet size and surface PEG density contributed to the NEs biological fate. It needs to be pointed out that the distinct tissue uptake by different formulations should be carefully extrapolate to the other animal models or human. Species-dependent organ

specificity for liposome was previously observed (Sou et al., 2011). The inter-species difference is largely attributed to the significant different circulation time, and this effect is amplified especially in the small rodents such as mice and rats as compared to hamster, rabbit and rhesus monkey. Another important physiological difference between animal models is the balance between organ/tissue to body weight ratio. Research has shown the spleen-to-body weight ratio of the rat is 3 times greater than that of the primate and 9 times greater than the that of the rabbit. This variation of mass balance of mononuclear phagocytic system (MPS) is therefore a crucial factor determining the biodistribution of liposomes between rats and rabbits (Sou et al., 2005).

Despite that the species difference should be scrutinized, yet the current study intrigues several potential follow-up research threads. First of all, it would be interesting to investigate the biological fate of small-size NE. Should SE truly end up in the bone marrow and lymphatic system, its containment in the circulatory system could be potentially useful in reducing systemic especially hepatic and renal toxicity of anticancer drugs in the treatment of blood-originated cancer such as leukemia and bone-related cancer. On the other hand, the favorable disposition of LE in the liver, spleen and lungs could be utilized as a size-dependent passive targeting strategy. Drugs which yield PD effect in these organs, such as Triclabendazole for fascioliasis and antibiotics for pulmonary infections, etc., could be encapsulated in LE for liver and lung targeted delivery, respectively. Secondly, for stage III liver and lung cancer, since the cancer has advanced to the nearby lymph nodes, the liver/lung targeting effect by LE could be possible to treat the whole organ and inhibit its distal metastasis. Further evaluation and comparison of the treatment efficacy of anticancer drug loaded ME and LE for liver/lung locally invaded tumor is hence desired to test the hypothesis. Notably, for these drug delivery purposes, LE should be optimized in such a way that the droplet size be reduced with wider size distributions acceptable for the improved formulation stability. Indeed, our preliminary results demonstrated that soybean lecithin

was an excellent NE stabilizer which simultaneously produce mean droplet size ranging from 300 to 500 nm. In this regard, the commercialized intravenous lipid nutrition could possibly serve the same purpose as the potential DDS for liver/lung targeted drug delivery. And lastly, the enhanced heart distribution by ME could similarly open up certain research potential for heart targeted delivery.

Appendices

The PK parameters from the current study were summarized in appendices. The parameters were obtained by non-compartmental analysis (NCA) with the aid of Phoenix® WinNonlin® (Certara, NJ). Linear trapezoidal and linear interpolation method with a uniform weighting were used to run the calculations. The PK parameters from DS, DSE, DME and DLE were summarized in **Table A.1** through **Table A.4**, respectively. **Figure A.1** illustrates the extent of the change in dose normalized DiI area under the curve ($AUC_{0\text{-}10h}$) in various tissues by DSE, DME and DLE versus DS, respectively. **Table A.5** compares DME and DLE by the ratio of plasma-normalized tissue $AUC_{0\text{-}10h}$ to show the intrinsic tissue affinity of the formulations.

Table A.1 Major apparent PK parameters in tissues followed by intravenous bolus administration of 5 mg/kg DiI in solution (DS) in C57BL/6J mice.

	C_{max} ($\mu g*mL^{-1}$ or $\mu g*g^{-1}$)	T_{max} (h)	$MRT_{0\text{-}10h}$ (h)	$MRT_{0\text{-}\infty}$ (h)	$AUC_{0\text{-}10h}$ ($\mu g*mL^{-1}*h$ or $\mu g*g^{-1}*h$)	$AUC_{0\text{-}\infty}$ ($\mu g*mL^{-1}*h$ or $\mu g*g^{-1}*h$)
Plasma	24.01	0.0	1.97	3.34	7.45	8.30
Heart	2.74	0.5	2.55	4.16	2.27	2.59
Liver	16.34	0.5	3.97	10.87	23.28	38.40
Spleen	32.68	0.5	3.77	8.45	35.92	51.05
Lung	15.52	0.25	3.17	4.18	14.49	15.93
Kidney	0.96	0.5	3.87	8.85	1.78	2.66
Stomach	0.30	0.5	4.75	8.47	1.62	2.31
Small Intestine	0.40	0.5	4.50	14.79	1.23	2.54
Colon	0.23	0.25	4.92	19.48	1.03	2.64
Tumor	0.39	0.5	4.79	19.22	1.12	2.81

Table A.2 Major apparent PK parameters in tissues followed by intravenous bolus administration of 2 mg/kg DiI in small-size nanoemulsion (DSE) in C57BL/6J mice.

	C_{max} (μg*mL^{-1} or μg*g^{-1})	T_{max} (h)	$MRT_{0\text{-}10h}$ (h)	$MRT_{0\text{-}\infty}$ (h)	$AUC_{0\text{-}10h}$ (μg*mL^{-1}*h or μg*g^{-1}*h)	$AUC_{0\text{-}\infty}$ (μg*mL^{-1}*h or μg*g^{-1}*h)
Plasma	19.23	0.0	2.32	15.57	5.80	10.66
Heart	0.74	0.25	4.28	45.01	1.52	7.14
Liver	1.44	0.25	5.43	N/A*	11.18	N/A
Spleen	1.13	0.25	5.41	N/A	5.99	N/A
Lung	0.48	0.25	4.76	68.59	1.56	11.38
Kidney	0.33	0.25	4.79	49.26	1.59	8.51
Stomach	0.25	4.0	5.50	N/A	1.86	N/A
Small Intestine	0.22	0.25	5.01	39.04	1.37	6.27
Colon	0.21	10.0	6.00	N/A	1.17	N/A
Brain	0.08	0.25	5.02	67.36	0.59	4.38
Tumor	0.16	0.25	5.46	N/A	1.01	N/A

*N/A: Not available.

Table A.3 Major apparent PK parameters in tissues followed by intravenous bolus administration of 5 mg/kg DiI in medium-size nanoemulsion (DME) in C57BL/6J mice.

	C_{max} (μg*mL^{-1} or μg*g^{-1})	T_{max} (h)	$MRT_{0\text{-}10h}$ (h)	$MRT_{0\text{-}\infty}$ (h)	$AUC_{0\text{-}10h}$ (μg*mL^{-1}*h or μg*g^{-1}*h)	$AUC_{0\text{-}\infty}$ (μg*mL^{-1}*h or μg*g^{-1}*h)
Plasma	29.19	0.0	3.92	9.01	79.69	120.25
Heart	10.01	1.0	4.76	32.57	50.33	192.91
Liver	20.65	10.0	5.97	N/A*	146.67	N/A
Spleen	31.03	4.0	5.58	N/A	198.67	N/A
Lung	37.39	0.5	4.58	5.19	128.58	138.80
Kidney	3.83	0.5	4.84	17.92	14.92	35.97
Stomach	2.35	0.5	5.31	69.78	10.34	82.98
Small Intestine	2.20	0.5	5.37	N/A	8.77	N/A
Colon	0.81	0.5	5.43	N/A	4.14	N/A
Brain	0.46	0.5	4.37	10.49	1.37	2.24
Tumor	3.01	10.0	7.01	N/A	11.88	N/A

*N/A: Not available.

Table A.4 Major apparent PK parameters in tissues followed by intravenous bolus administration of 5 mg/kg DiI in large-size nanoemulsion (DLE) in C57BL/6J mice.

	C_{max} ($\mu g*mL^{-1}$ or $\mu g*g^{-1}$)	T_{max} (h)	MRT_{0-10h} (h)	$MRT_{0-\infty}$ (h)	AUC_{0-10h} ($\mu g*mL^{-1}*h$ or $\mu g*g^{-1}*h$)	$AUC_{0-\infty}$ ($\mu g*mL^{-1}*h$ or $\mu g*g^{-1}*h$)
Plasma	39.43	0.0	2.11	2.21	66.76	67.39
Heart	5.63	2.0	2.55	2.65	18.10	18.29
Liver	28.91	2.0	2.96	3.09	126.65	128.50
Spleen	69.44	2.0	2.73	2.76	220.79	221.46
Lung	41.53	2.0	2.48	2.48	140.41	140.55
Kidney	4.85	2.0	2.71	2.83	14.57	14.76
Stomach	1.50	2.0	2.90	3.47	5.88	6.22
Small Intestine	1.11	0.5	3.12	4.19	4.09	4.52
Colon	0.97	0.5	3.34	4.97	2.81	3.28
Brain	0.66	0.5	3.00	4.00	1.60	1.76
Tumor	2.27	2.0	2.80	3.07	6.62	6.81

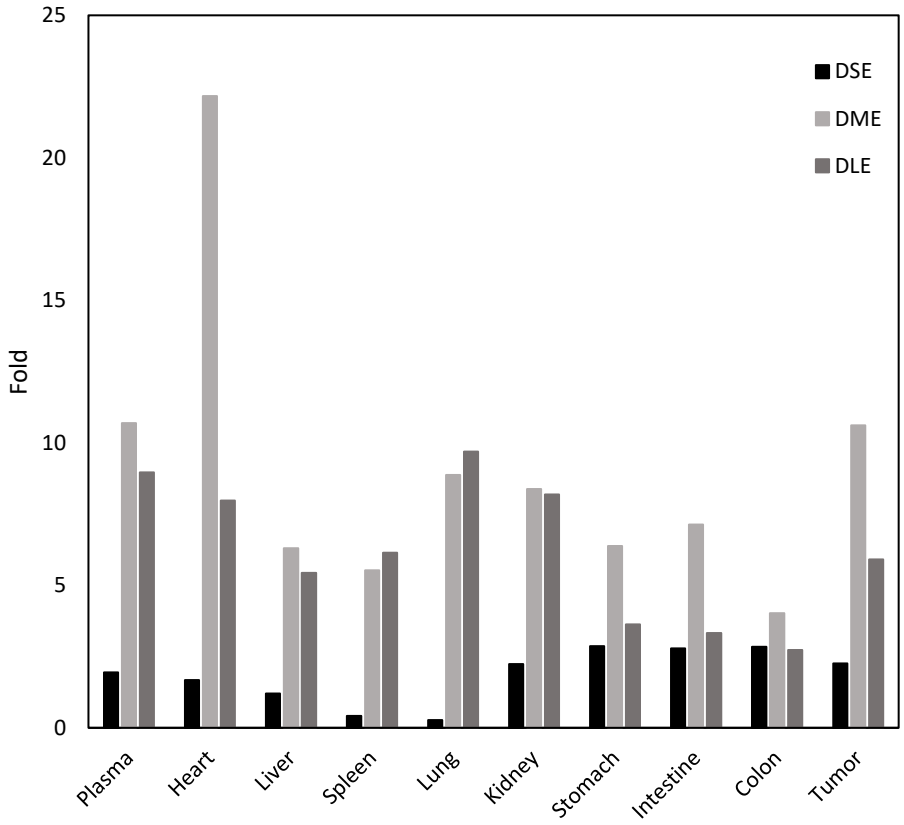

Figure A.1 The comparison of dose normalized DiI apparent area under the curve ($AUC_{0\text{-}10h}$) in various tissues after intravenous bolus injection of DiI loaded small-, medium- and large-size nanoemulsion (DSE, DME and DLE) versus DiI solution (DS), respectively.

Table A.5 The ratio of plasma-normalized tissue apparent $AUC_{0\text{-}10h}$ by DME versus DLE

Tissue	Plasma normalized $AUC_{0\text{-}10h}$		Normalized ratio
	DME	DLE	
Plasma	N/A*	N/A	N/A
Heart	0.653	0.293	2.23
Liver	1.902	2.048	0.93
Spleen	2.493	3.307	0.75
Lung	1.667	2.271	0.73
Kidney	0.193	0.236	0.82
Stomach	0.134	0.095	1.41
Intestine	0.114	0.066	1.73
Colon	0.054	0.045	1.20
Brain	0.018	0.026	0.69
Tumor	0.154	0.107	1.44

* N/A: Not applicable.

References

Alexis, F., Pridgen, E., Molnar, L.K. and Farokhzad, O.C. Factors affecting the clearance and biodistribution of polymeric nanoparticles. *Molecular Pharmaceutics*. 5 (2008) 4:505-515. doi: 10.1021/mp800051m.

Ali, S. and Kolter K. Kolliphor® HS 15 - An enabler for parenteral and oral formulations. *American Pharmaceutical Review*. 22 (2019) 1:22-34.

Aschoff, L. Das reticulo-endotheliale System. Ergebnisse der Inneren Medizin und Kinderheilkunde: Sechsundzwanzigster Band (in German). Springer Berlin Heidelberg: 1–118. doi:10.1007/978-3-642-90639-8_1.

Astruc, D. Introduction to nanomedicine. *Molecules* 21 (2016) 4:1-6. doi:10.3390/molecules21010004.

Attia, M.F., Anton, N., Akasov, R., Chiper, M., Markvicheva, E. and Vandamme, T.F. Biodistribution and toxicity of X-ray iodinated contrast agent in nano-emulsions in function of their size. *Pharm Res*. 33 (2016) 3:603-614. doi: 10.1007/s11095-015-1813-0.

Avgoustakis, K., Beletsi, A., Panagi, Z., Klepetsanis, P., Livaniou, E., Evangelatos, G., Ithakissios, D.S. Effect of copolymer composition on the physicochemical characteristics, in vitro stability, and biodistribution of PLGA–mPEG nanoparticles. *International Journal of Pharmaceutics*. 259 (2003) 115–127.

Alexander, J., Dainiak, N., Berger, H.J., Goldman, L., Johnstone, D., Reduto, L., Duffy, T., Schwartz, P., Gottschalk, A., Zaret, B.L. and Pytlik, L. Serial Assessment of Doxorubicin Cardiotoxicity with Quantitative Radionuclide Angiocardiography. *N Engl J Med*. 300 (1979) 278-283. DOI: 10.1056/NEJM197902083000603.

Baas, J., Senninger, N. and Elser, H. The reticuloendothelial system. An overview of function, pathology and recent methods of measurement. *Z Gastroenterol*. 32 (1994) 2:117-23.

Bittner, B., Gonzalez, R.B., Walter, I., Kapps, M. and Huwyler, J. Impact of Solutol HS 15 on the pharmacokinetic behaviour of colchicine upon intravenous administration to male wistar rats. *Biopharm. Drug Dispos*. 24 (2003) 173–181.

Bouchemal, K., Briançon, S., Perrier, E. and Fessi, H. Nano-emulsion formulation using spontaneous emulsification: solvent, oil and surfactant optimisation, *Int. J. Pharm*. 280 (2004) 241–251.

Blanco, E., Shen, H. and Ferrari, M. Principles of nanoparticle design for overcoming biological barriers to drug delivery. *Nat Biotechnol*. 33 (2015) 9:941–951. doi:10.1038/nbt.3330.

Braet, F., Wisse, E., Bomans, P., Frederik, P., Geerts, W., Koster, A., Soon, L. and Ringer, S. Contribution of high-resolution correlative imaging techniques in the study of the liver sieve in three-dimensions. *Microsc Res Tech*. 70 (2007) 230–242. https://doi.org/10.1002/jemt.20408.

Brelje, T.C., Wessendorf, M.W. and Sorenson R.L. *Methods in cell biology*. 38 (1993) 97-181. https://doi.org/10.1016/S0091-679X(08)61001-8.

Buszello, K., Harnisch, S., Muller, R.H. and Muller, B.W. The influence of alkali fatty acids on the properties and the stability of parenteral o/w emulsions modified with Solutol HS 15. *European Journal of Pharmaceutics and Biopharmaceutics* 49 (2000) 143-149.

Chen, G., He, Z., Yu, X., Wang, T., Gao, C., Song, L., Wu, H., Yin, C., Luo, S., Zhang, Y. and Gu, N. Size-dependent biodistribution of iodinated oil nanoemulsions observed by dual-modal imaging in rats. *J Nanosci Nanotechnol* (2016) Mar;16(3):2474-81.

Chen, L.T. and Weiss L. The role of the sinus wall in the passage of erythrocytes through the spleen. *Blood*. 41 (1973) 529–537.

Choi, H.S., Liu, W., Misra, P., Tanaka, E., Zimmer, J.P., Itty Ipe, B., Bawendi, M.G. and Frangioni, J.V. Renal clearance of quantum dots. *Nat Biotechnol*. 25 (2007) 1165–1170.

Cooper, J.T. and Harris, J.M. Imaging fluorescence-correlation spectroscopy for measuring fast surface diffusion at liquid/solid interfaces. *Anal. Chem*. (2014), 86, 15, 7618-7626. http://doi: 10.1021/ac5014354.

Croce, A.C. and Bottiroli, G. Autofluorescence spectroscopy and imaging: a tool for biomedical research and diagnosis. *European Journal of Histochemistry*. (2014) 58:2461; 320-337. http://doi: 10.4081/ejh.2014.2461.

Cumming, J.D. A study of blood flow through bone marrow by a method of venous effluent collection. *J. Physiol.* 162 (1962) 13-20.

Danaei, M., Dehghankhold, M., Ataei, S., Davarani, F.H., Javanmard, R., Dokhani, A., Khorasani, S. and Mozafari, M.R. Impact of particle size and polydispersity index on the clinical applications of lipidic nanocarrier systems. *Pharmaceutics*. 10 (2018) 57; doi:10.3390/pharmaceutics10020057.

Delmas, T., Piraux, H., Couffin, A.C., Texier, I., Vinet, F., Poulin, P., Cates, M.E. and Bibette J. How to prepare and stabilize very small nanoemulsions. *Langmuir* 2011, 27(5), 1683–1692.

Endepols, H., Jungnickel, J. and Braun K. Physiological and morphological characterization of organotypic cocultures of the chick forebrain area MNH and its main input area DMA/DMP. *Neural Plasticity*. 8 (2001) 219-240. http:// doi: 10.1155/NP.2001.219.

Ernsting, M.J., Murakami, M., Roy, A. and Li, S. Factors controlling the pharmacokinetics, biodistribution and intratumoral penetration of nanoparticles. *J Control Release*. 172 (2013) 3:782-794. http://doi:10.1016/j.jconrel.

European Science Foundation. Forward Look Nanomedicine: An EMRC Consensus Opinion 2005.

Fallatah, W., De Silva, I.W., Verbeck, G.F. and r Jagadeeswaran, P. Generation of transgenic zebrafish with 2 populations of RFP- and GFP-labeled thrombocytes: analysis of their lipids. *Blood Advances*. 3 (2019) 1406-1415. http://doi: 10.1182/bloodadvances.2018023960.

Fernandez, P., André, V., Rieger, J. and Kühnle, A. Nano-emulsion formation by emulsion phase inversion. *Colloids Surf. A Physicochem. Eng. Asp*. 251 (2004) 53–58.

Gelderblom, H., Verweij, J., Nooter, K., Sparreboom, A. Cremophor EL: the drawbacks and advantages of vehicle selection for drug formulation. *European Journal of Cancer* 37 (2001) 1590–1598.

Gjedde, S.B. and Gjedde, A. Organ blood flow rates and cardiac output of the Balb/c mouse. *Comp. Biochem. Physiol.* 67A (1980) 671-674.

Gref, R., Domb, A., Quellec, P., Blunk, T., Muller, R.H., Verbavatz, J.M., Langer, R. The controlled intravenous delivery of drugs using PEG-coated sterically stabilized nanospheres. *Advanced Drug Delivery Reviews*. 16 (1995) 215-233.

Gupta, A., Eral, H.B., Hatton, T.A. and Doyle, P.S. Nanoemulsions: formation, properties and applications. *Soft Matter*. 2016 12(11):2826-41. DOI: 10.1039/c5sm02958a.

Hagigit, T., Abdulrazik, M., Orucov, F., Valamanesh, F., Lambert, M., Lambert, G., Behar-Cohen, F. and Benita, S. Topical and intravitreous administration of cationic nanoemulsions to

deliver antisense oligonucleotides directed towards VEGF KDR receptors to the eye. *J. Control. Release* 145 (2010) 297–305.

Hak, S., Garaiova, Z., Olsen, L.T., Nilsen, A.M., Davies, C.L. The Effects of oil-in-water nanoemulsion polyethylene glycol surface density on intracellular stability, pharmacokinetics, and biodistribution in tumor bearing mice. *Pharm Res* 32 (2015) 1475–1485. DOI 10.1007/s11095-014-1553-6.

Hammond, E.G., Johnson, L.A., Su, C., Wang, T. and White, P.J. *Bailey's Industrial Oil and Fat Products (Sixth Edition)*. (2005) Chapter 13. Soybean oil.

Harris, J.M., Martin, N.E. and Modi, M. Pegylation: a novel process for modifying pharmacokinetics. *Clin Pharmacokinet*. 40 (2001) 7:539-551.

Honig, M.G. and Hume, R.I. Dil and DiO: versatile fluorescent dyes for neuronal labelling and pathway tracing. *Trends Neurosci*. 12 (1989) 9:333-5, 340-1. https://doi.org/10.1016/0166-2236(89)90040-4.

He, C., Hu, Y. Yin, L., Tang, C. and Yin, C. Effects of particle size and surface charge on cellular uptake and biodistribution of polymeric nanoparticles. *Biomaterials*. 31 (2010) 3657-3666.

He, H., Liu, L., Morin, E.E., Liu, M. and Schwendeman, A. Survey of clinical translation of cancer nanomedicines-Lessons Learned from successes and failures. *Acc. Chem. Res*. 52 (2019) 2445−2461.

Hippalgaonkar, K., Majumdar, S., and Kansara V. Injectable lipid emulsions - Advancements, opportunities and challenges. *AAPS PharmSciTech.* 11 (2010) 1526-1540.

Honig, M.G., Hume, R.I. Fluorescent carbocyanine dyes allow living neurons of identified origin to be studied in long-term cultures. *J Cell Biol* 103 (1986) 1:171–187. https://doi.org/10.1083/jcb.103.1.171.

Huang, T.S. Passage of foreign particles through the sinusoidal wall of the rabbit bone marrow – an electron microscopic study. *Acta Pathol Jpn*. 21 (1971) 3:349-367, ISSN 0001-6632.

Huang, X., Xu, Q. and Jeffrey, R. Rapid and sensitive determination of Rhodamine B in cosmetics. (2016) *Thermo Fisher Scientific* Application Note 1102.

Imasaka, T., Kadone, H., Ogawa, T. and Ishibashi, N. Detection limit of fluorescein as determined by fluorometry with an esculin laser source. *Analytical Chemistry* 49 (1977) 4: 667-668.

Invitrogen (2010) In "Molecular Probes™ Handbook: A Guide to Fluorescent Probes and Labeling Technologie", 11th Ed. pp. 589-648. Thermo Fisher Scientific.

Jeansson, M. and Haraldsson, B. Glomerular size and charge selectivity in the mouse after exposure to glucosaminoglycan-degrading enzymes. *J Am Soc Nephrol* 14 (2003) 1756–1765.

Kaliss, N. and Pressman D. Plasma and blood volumes of mouse organs, as determined with radioactive iodoproteins. *Proc Soc Exp Biol Med*. 75 (1950) 1:16-20.

Kety, S.S. and Schmidt, C.F. The effects of active and passive hyperventilation on cerebral blood flow, cerebral oxygen consumption, cardiac output, and blood pressure of normal young men. *J. clin. Invest.* 25 (1946) 107-119.

Kim, K., Choi, B., Park, S., Lee, S., Christensen, L.V., Zhou, J., Shin, B.Y., Bae, K., Kern, S.E., Kang, S. and Noh, G. Pharmacokinetics and pharmacodynamics of propofol microemulsion and

lipid emulsion after an intravenous bolus and variable rate infusion. *Anesthesiology*. 106 (2007) 926-934.

Kola, I. and Landis, J. Can the pharmaceutical industry reduce attrition rates? *Nature Reviews Drug Discovery*. 3 (2004) 711–716.

Levick, J.R. and Smaje, L.H. An analysis of the permeability of a fenestra. *Microvasc Res* 33 (1987) 233–256. [PubMed: 3587078]

Liu, D., Mori, A. and Huang, L. Role of liposome size and RES blockade in controlling biodistribution and tumor uptake of GM_1-containing liposomes. *Biochimica et Biophysica Acre*, 1104 (1992) 95-101.

Lu, H., Li, J., Li, M., Gong, T. and Zhang, Z. Systemic delivery of alpha-asarone with Kolliphor HS 15 improves its safety and therapeutic effect on asthma. *Drug Delivery*. 22 (2015) 3:266-75.

Ma, M., Hao, Y., Liu, N., Yin, Z., Wang, L., Liang, X. and Zhang, X. A novel lipid-based nanomicelle of docetaxel: evaluation of antitumor activity and biodistribution. *International Journal of Nanomedicine*. 7 (2012) 3389–3398.

Ma, Y., Sadoqi, M. and Shao, J. Biodistribution of indocyanine green-loaded nanoparticles with surface modifications of PEG and folic acid. *International Journal of Pharmaceutics* 436 (2012) 25– 31.

Madea, H., Nakamura, H. and Fang, J. The EPR effect for macromolecular drug delivery to solid tumors: Improvement of tumor uptake, lowering of systemic toxicity, and distinct tumor imaging in vivo. *Advanced Drug Delivery Reviews* 65 (2013) 71–79.

Mason,T.G.,Wilking, J., Meleson, K., Chang, C., and Graves, S. Nanoemulsions: formation, structure, and physical properties. *J. Phys. Condens. Matter*. 18 (2006) R635.

Matsumura, Y. and Maeda, H. A New Concept for Macromolecular Therapeutics in Cancer Chemotherapy: Mechanism of Tumoritropic Accumulation of Proteins and the Antitumor Agent Smancs. *Cancer Research* 46 (1986) 6387-6392.

McClements, D.J. Nanoemulsions versus microemulsions: terminology, differences, and similarities. *Soft Matter.* 8 (2012) 1719-1729.

Moghimi, S.M. Exploiting bone marrow microvascular structure for drug delivery and future therapies. *Adv Drug Deliv Rev*. 17 (1995) 1:61–73, ISSN 0169-409X.

Nicholas, J.W. and Bae, Y.H. EPR: Evidence and fallacy. *J Control Release*. 190 (2014) 451-464. doi: 10.1016/j.jconrel.2014.03.057.

Oliveira, H., Thevenot, J., Garanger, E., Ibarboure, E., Calvo, P., Aviles, P., Guillen, MJ., Lecommandoux, S. Nano-encapsulation of Plitidepsin: In vivo pharmacokinetics, biodistribution, and efficacy in a renal xenograft tumor model. *Pharm Res* 31 (2014) 983–991.

Overwijk, W.W., Restifo, N.P. B16 as a mouse model for human melanoma. *Curr Protoc Immunol*. (2001) Chapter: Unit–20.1. doi:10.1002/0471142735.im2001s39.

Papahadjopoulos, D, Allen, T.M., Gabizon, A., Mayhew, E., Matthay, K., Huang, S.K., Lee, K.D., Woodle, M.C., Lasic, D.D., Redemann, C. and Martin, F.J. Sterically stabilized liposomes: Improvements in pharmacokinetics and antitumor therapeutic efficacy. *Proc. Natl. Acad. Sci.* 88 (1991) 11460-11464.

Peer, D., Karp, J.M., Hong, S., Farokhzad, O.C., Margalit, R., Langer, R. Nanocarriers as an emerging platform for cancer therapy. *Nat. Nanotechnol*. 2 (2007) 751–760.

Perrault S.D., Walkey C., Jennings T., Fischer H.C., Chan W.C.W. Mediating tumor targeting efficiency of nanoparticles through design. *Nano Lett.* 9 (2009) 1909-1915.

Popović Z., Liu W., Chauhan V.P. A nanoparticle size series for in vivo fluorescence imaging. *Angew. Chem. Int. Ed. Engl.* 49 (2010) 8649-8652.

Porter, C.J., Moghimi, S.M., Illum, L. and Davis, S.S. The polyoxyethylene/polyoxypropylene block co-polymer poloxamer-407 selectively redirects intravenously injected microspheres to sinusoidal endothelial cells of rabbit bone marrow. *FEBS Lett*. 305 (1992) 1:62-66, ISSN 0014-5793.

Pozzi, D., Colapicchioni, V., Caracciolo, G., Piovesana, S., Capriotti, A.L., Palchetti, S., Grossi, S.D., Riccioli, A., Amenitsch, H. and Lagana, A. Effect of polyethyleneglycol (PEG) chain length on the bio–nano-interactions between PEGylated lipid nanoparticles and biological fluids: from nanostructure to uptake in cancer cells. *Nanoscale*. 6 (2014) 2782–2792. DOI: 10.1039/c3nr05559k.

Prabhakar, U., Maeda, H., Jain, R.K., Sevick-Muraca,E.M., Zamboni, W., Farokhzad6, O.C., Barry, S.T., Gabizon, A., Grodzinski1, P. and Blakey, D.C. Challenges and key considerations of the enhanced permeability and retention (EPR) effect for nanomedicine drug delivery in oncology. *Cancer Res*. 73 (2013) 8:2412–2417. http://doi:10.1158/0008-5472.CAN-12-4561.

Product monograph for INTRALIPID® lipid injectable emulsion, Mfr. Std. Soybean Oil 10%, 20%, 30% w/v lipid emulsions for intravenous nutrition.

Reisch, A. and Klymchenko, A.S. Fluorescent polymer nanoparticles based on dyes: seeking brighter tools for bioimaging. *Small*. 12 (2016) 15:1968–1992. http://doi:10.1002/smll.201503396.

Risau, W. Development and differentiation of endothelium. *Kidney Int Suppl* 67 (1998) S3–S6. [PubMed: 9736244].

Rivera, G.P., Hühn, D., del Mercato, L.L., Sasse, D. and Parak, W.J. Nanopharmacy: Inorganic nanoscale devices as vectors and active compounds. *Pharmacol Res*. 62 (2010) 2:115-125.

Robert, W.G. and Palade, G.E. Endothelial fenestrae and fenestral diaphragms. *Morphogenesis of Endothelium*, edited by Risau W and Rubanyi GM. Amsterdam, The Netherlands: Harwood Academic. (2000) p.23–41.

Saba, T.M. Physiology and physiopathology of the reticuloendothelial system. *Arch Intern Med.* 126 (1970) 1031-1052.

Scheller, A. and Kirchhoff, F. Endocannabinoids and heterogeneity of glial cells in brain function. *Frontiers in Integrative Neuroscience*. 10 (2016) 24: 1-6. doi: 10.3389/fnint.2016.00024.

Schettini, D.A., Ribeiro, R.R., Demicheli, C., Rocha, O.G., Melo, M.N., Michalick, M.S. and Frézard, F. Improved targeting of antimony to the bone marrow of dogs using liposomes of reduced size. *Int J Pharm*. 315 (2006) 1-2: 140-147, ISSN 0378-5173.

Shah, S.m., Jain, A.S., Kaushik, R., Nagarsenker, M.S. and Nerurkar, M.J. Preclinical formulations: Insight, strategies, and practical considerations. *AAPSSciTech*. 15 (2014) 1307-1322.

Shobhit, K., Javed, A. and Sanjula, B. Design Expert ® supported optimization and predictive analysis of selegiline nanoemulsion via the olfactory region with enhanced behavioral performance in Parkinson's disease. *Nanotechnology* 27 (2016) 435101.

Simon, C.S. and Filip, B. Glomerular endothelial cell fenestrations: an integral component of the glomerular filtration barrier. *Am J Physiol Renal Physiol*. 296 (2009) 5:947-956.

Singh, Y., Meher, J.G., Raval, K., Khan, F.A., Chaurasia, M., Jain, N.K., Chaurasia, M.K. Nanoemulsion: Concepts, development and applications in drug delivery. *Journal of Controlled Release* 252 (2017) 28–49.

Soliman, K.A, Ibrahim, H.K. and Ghorab, M.M. Formulation of avanafil in a solid-selfnanoemulsifying drug delivery system for enhanced oral delivery. *Eur. J. Pharm. Sci.* 93 (2016) 447–455.

Sou, K., Goins, B., Oyajobi, B.O., Travi, B.L. and Phillips, W.T. Bone marrow-targeted liposomal carriers. *Expert Opin Drug Deliv*. 8 (2011) 3: 317–328. doi:10.1517/17425247.2011.553218.

Sou, K., Klipper, R. and Goins, B. Circulation kinetics and organ distribution of Hb-vesicles developed as a red blood cell substitute. *J Pham Exp Ther*. 312 (2005) 702-709.

Süel, G. Use of fluorescence microscopy to analyze genetic circuit dynamics. *Methods in enzymology*. 497 (2011) 275-293. https://doi.org/10.1016/B978-0-12-385075-1.00013-5.

Suzuki, Y. and Yokoyama, K. Development of functional fluorescent molecular probes for the detection of biological substances. *Biosensors (Basel)*. 5 (2015) 2:337–363. https://doi:10.3390/bios5020337.

Tansi,F.L., Rüger, R., Rabenhold, M., Steiniger, F., Fahr, A. and Hilger, I. Fluorescence-quenching of a liposomal-encapsulated near-infrared fluorophore as a tool for in vivo optical imaging. *J Vis Exp*. 95 (2015) 52136. http://doi: 10.3791/52136.

Tomayko M.M. and Reynolds C.P. Determination of subcutaneous tumor size in athymic (nude) mice. *Cancer Chemother Pharmacol*. 1989;24(3):148-54.

Venkateshwarlu, I., Prabhakar, K., Ali, M. and Kishan, V. Development and in vitro cytotoxic evaluation of parenteral docetaxel lipid nanoemulsions for application in cancer treatment. *PDA J. Pharm. Sci. Technol.* 64 (2010) 233–241.

Ventola, C.L. Progress in Nanomedicine: Approved and Investigational Nanodrugs. *P&T*. 42 (2017) 742-755.

Wang, S.W., Monagle, J., McNulty, C., Putnam, D. and Chen, H. Determination of P-glycoprotein inhibition by excipients and their combinations using an integrated high-throughput process. *J. Pharm. Sci*. 93 (2004) 2755-2767.

Wei, B., He, M., Cai, X., Hou, X., Wang, Y., Chen, J., Lan, M., Chen, Y., Lou, K. and Gao, F. Vitamin E succinate-grafted-chitosan/chitosan oligosaccharide mixed micelles loaded with C-DMSA for Hg2+ detection and detoxification in rat liver. *Int J Nanomedicine*. 14 (2019) 6917–6932. http://doi: 10.2147/IJN.S213084.

Wells, K.S., Sandison, D.R., Strickler, J. and Webb, W.W. (1990) In "Handbook of Biological Confocal Microscopy" (J. B. Pawley, ed.), 2nd Ed., pp. 27-39. Plenum, New York.

Wen, Z., Muratomi, N., Huang, W., Huang, L., Ren, J., Yang, J., Persaud, Y., Loloi, J., Mallangada, N., Kung, P., Honkanen, R. and Rigas, B. The ocular pharmacokinetics and biodistribution of phospho-sulindac (OXT-328) formulated in nanoparticles: Enhanced and targeted tissue drug delivery. *International Journal of Pharmaceutics* 557 (2019) 273–279.

Xu, Q., Buhler, E., Steinmetz, A., Schonitzer, D., Bock, G., Jurgens, G. and Wick, G. A high-density-lipoprotein receptor appears to mediate the transfer of essential fatty acids from high-density lipoprotein to lymphocytes. *Biochem. J.* 287 (1992) 395-40. http://doi: 10.1042/bj2870395.

Yilmaz, E. and Borchert, H.H. Design of a phytosphingosine-containing, positivelycharged nanoemulsion as a colloidal carrier system for dermal application of ceramides. *Eur. J. Pharm. Biopharm*. 60 (2005) 91–98.

Vita

Name	*Jiayi Chen*
Baccalaureate Degree	*Bachelor of Medicine, Fudan University, Shanghai*
	Major: Clinical Medicine
Date Graduated	*July, 2008*
Other Degrees and Certificates	*Master of Science, St. John's University, New York*
	Major: Industrial Pharmacy
Date Graduated	*December, 2012*